Modelling the deep convective transport of trace gases (CO, NH₃ and SO₂) from the planetary boundary layer to the Asian summer monsoon anticyclone

Jianzhong Ma[1,2,3], Bin Chen[1], Qianshan He[4], Xiaolu Yan[1,2], Gaili Wang[1,3,5], Siyang Cheng[1,2,3], Benedikt
Steil[6], Christoph Brühl[6], Andrea Pozzer[6], and Jos Lelieveld[6]

[1]Institute of Tibetan Plateau Meteorology & State Key Laboratory of Severe Weather Meteorological Science and Technology,
Chinese Academy of Meteorological Sciences, Beijing 100081, China
[2]Heavy Rain and Drought-Flood Disasters in Plateau and Basin Key Laboratory of Sichuan Province, Institute of Tibetan
Plateau Meteorology, China Meteorological Administration, Chengdu 610213, China
[3]Mêdog National Climate Observatory & Mêdog Field Research Station for Atmospheric Water Cycle, China Meteorological
Administration, Linzhi 860700, China
[4]Shanghai Meteorological Service & Shanghai Key Laboratory of Meteorology and Health, Shanghai 201199, China
[5]Mêdog Atmospheric Water Cycle Observation and Research Station of Xizang Autonomous Region, Linzhi, 860700, China
[6]Atmospheric Chemistry Department, Max Planck Institute for Chemistry, Mainz, Germany

Correspondence to: Jianzhong Ma (majz@cma.gov.cn)

Abstract. Deep convection plays a vital role in transporting Asian pollutants from the planetary boundary layer (PBL) into the
Asian summer monsoon anticyclone (ASMA). However, the efficiency and effectiveness of transporting pollutants with
various chemical and physical properties to the ASMA remain unclear. In this study, we use the global atmospheric chemistry
and climate model EMAC to investigate the deep convective transport of trace gases such as CO, NH₃ and SO₂ from the PBL
to the ASMA over the years 2010-2020. We quantify the deep convective transport efficiency of different trace gases into the
ASMA. We show that the strongest convective transport tendency occurs over northern India and the southern edge of the
Tibetan Plateau for CO (0.2-0.5 ppbv hr^{-1}), over the south and eastern parts of the Tibetan Plateau for NH₃ (0.02-0.05 ppbv
hr^{-1}), and over central India and eastern China for SO₂ (0.002-0.005 ppbv hr^{-1}). We find that, in contrast to CO and NH₃, the
SO₂ enhancements within the ASMA are very weak, and there is can even be a decrease in SO₂ over the southern Tibetan
Plateau relative to the surroundings. Our analysis indicates that gas-liquid partitioning in clouds and subsequent wet deposition
over South Asia are more effective at reducing SO₂ than NH₃ reaching the Tibetan Plateau and the ASMA. In view of ongoing
changes in regional emissions, the effects of deep convective transport of various pollutants and associated gas-aerosol-cloud
interactions on the chemical features of the ASMA require continued investigation.

1 Introduction

Deep convection plays an important role in the vertical redistribution of trace gases and the pollution transport from the planetary boundary layer (PBL) to the upper troposphere and lower stratosphere (UTLS) (Chatfield and Crutzen, 1984;Dickerson et al., 1987;Lelieveld and Crutzen, 1994). The rapid transport of reactive pollutants from the PBL to the free troposphere and the tropopause region can significantly impact the UTLS chemistry globally (Pickering et al., 1990;Thompson et al., 1994;Thornton et al., 1997;Barth et al., 2007;Bertram et al., 2007;Barth et al., 2012). The deep and widespread convection associated with the Asian summer monsoon is a convective manifestation observed in June, July, and August that is absent in the Northern Hemisphere wintertime (Houze Jr. et al., 2015). Deep convection can transport Asian pollutants, especially those from South Asia, to the Asian summer monsoon anticyclone (ASMA) (Hoskins and Rodwell, 1995), where they are confined by the ASMA flow, forming a distinct chemical regime in the UTLS of the Northern Hemisphere during summertime (Randel and Park, 2006;Park et al., 2007;Park et al., 2008;Randel et al., 2010). The strength of the barrier separating air masses inside and outside the anticyclone depends on altitude, and there are also daily and yearly variations of the ASMA in relation to its boundary, area, and dynamic behaviour (Ploeger et al., 2015;Kachula et al., 2025). Satellite observations have revealed increasing levels of tropospheric gases (e.g., CO, HCN and NH_3) within the ASMA relative to outside it (Kar et al., 2004;Randel et al., 2010;Höpfner et al., 2016;Santee et al., 2017). A widespread strong enhancement of aerosols within the ASMA, namely the Asian Tropopause Aerosol Layer (ATAL), has also been detected by satellites (Vernier et al., 2011;Thomason and Vernier, 2013;Vernier et al., 2015).

The ASMA can serve as "an efficient smokestack" venting Asian surface pollutants to the global stratosphere (Yu et al., 2017;Bian et al., 2020). While the central role of the ASMA is recognized, there is still inconsistency about the most efficient pathway for the transport of moisture and air pollutants to the UTLS (Chen et al., 2012;Chen et al., 2024). The Tibetan Plateau plays a critical role in transporting air pollutants from the lower troposphere to the stratosphere during the Asian summer monsoon (Zhou et al., 1995). Deep convection over the Tibetan Plateau and its southern slope is considered "a short circuit" for the transport of water vapor and polluted air to the global stratosphere (Li et al., 2005;Fu et al., 2006). The middle troposphere centered over the southern Tibetan Plateau can act as "a well-defined conduit", where strong convection lofts air parcels in the boundary layer into the ASMA (Bergman et al., 2013;Bian et al., 2020). In addition, the northern Bay of Bengal and adjacent land area, where air pollution from the Indian subcontinent converges, has been identified as the central aerosol-convection source area for the ATAL (e.g., Park et al., 2009;Fadnavis et al., 2013;He et al., 2021;Nützel et al., 2022). The emissions from South Asia have been shown to make a dominant contribution to gaseous and aerosol pollutants trapped in the ASMA (Bergman et al., 2013;Lelieveld et al., 2018;Ma et al., 2022). While SO_2 and NO_2 emissions in India have been observed to increase rapidly (Krotkov et al., 2016), how these South Asian pollutants are transported to the ASMA and how they affect its chemical features remains an area in need of in-depth investigation.

The ASMA constitutes a seasonally persistent, zonally restricted circulation pattern transporting climate-relevant emissions rapidly from surface sources to higher altitudes (Vogel et al., 2015;Vogel et al., 2016;Ploeger et al., 2017;Vogel et al., 2023).

Transport by deep convection generally occurs alongside scavenging and multiphase chemical reactions involving reactive trace gases and aerosols, and it is also accompanied by various gas-aerosol-cloud interactions (Iribarne and Pyshnov, 1990;Pruppacher and Klett, 1997;Zondlo et al., 1997;Seinfeld and Pandis, 2006;Bertram et al., 2007). In addition to the convective dynamic activity, the deep convective transport efficiency of air pollutants, which reflects the amount of gases or aerosols reaching the outflow at the cloud top relative to that of the inflow into the convective mass near the cloud base, can change significantly with the difference in their solubility, hydrophilicity and reactivity (Barth et al., 2007;Barth et al., 2015;Yang et al., 2015;Bela et al., 2016). Therefore, understanding the various physical and chemical processes involved in the deep convective transport is essential for revealing the chemical characteristics of air masses within the ASMA and the formation mechanism of the ATAL. Several measurement campaigns have been conducted successfully to explore the chemical composition and spatiotemporal distributions of air pollutants in the UTLS over the Asian summer monsoon region, including the High Altitude and Long Range Research Aircraft (HALO) measurement (e.g., Gottschaldt et al., 2017), the Oxidation Mechanism Observations (OMO) campaign (Lelieveld et al., 2018;Hottmann et al., 2020), the Balloon Measurements of the Asian Tropopause Aerosol Layer (BATAL) (Vernier et al., 2018;Vernier et al., 2022), the StratoClim field campaign (Höpfner et al., 2019;Johansson et al., 2020;Lee et al., 2021;von Hobe et al., 2021;Appel et al., 2022;Singer et al., 2022;Ebert et al., 2024;Johansson et al., 2024), the Asian Summer Monsoon Chemical and CLimate Impact Project (ACCLIP) (e.g., Smith et al., 2025), and the Probing High Latitude Export of Air from the Asian Summer Monsoon (PHILEAS) campaign (Riese et al., 2025;Vogel et al., 2025). However, these measurements in Asia have still not fully characterized and quantified the deep convective transport of air pollutants from the PBL to the ASMA, compared to the Deep Convective Clouds and Chemistry (DC3) field experiment taking place in North America (e.g., Barth et al., 2015).

In the present study, we use the ECHAM/MESSy Atmospheric Chemistry (EMAC) model (Jöckel et al., 2006;Jöckel et al., 2010) to investigate the deep convective transport of trace gases, including carbon monoxide (CO), ammonia (NH_3) and sulfur dioxide (SO_2), from the PBL to the ASMA. CO is a typical pollution tracer that is transported into and trapped within the ASMA (Fu et al., 2006;Park et al., 2007). NH_3 and SO_2 have a much higher solubility and reactivity in water clouds than CO, and can act as gaseous precursors of ammonium sulfate aerosols (Seinfeld and Pandis, 2006). Therefore, deep convective transport of NH_3 and SO_2 from the PBL to the ASMA may significantly influence the formation processes and chemical composition of the ATAL (Höpfner et al., 2019). There is substantial interannual variability in the ASMA. For example, in summer 2015, the monsoon, in particular upward transport in the ASMA, was strongly influenced by El Niño, which has a global impact lasting over many months (Kunze et al., 2016;Santoso et al., 2017;Yan et al., 2018;Fadnavis et al., 2019;Ravindra Babu et al., 2021;Becker et al., 2025). Further, the composition of the ASMA tends to have strong day-to-day variability, influenced by various meteorological conditions such as typhoons (Vogel et al., 2014;Hanumanthu et al., 2020;Li et al., 2020;Li et al., 2021;Li et al., 2023). For this study, we performed model simulations using EMAC for a relatively long period, from January 2010 through December 2020. This study aims to investigate the deep convective transport of selected trace gases to the ASMA for a climatology of 2010-2020.

This paper is organized as follows. In Sect. 2, we describe the EMAC model and settings used for this study. In Sect. 3, we present the model simulation results, including the tendency and efficiency of the deep convective transport of CO, NH_3 and SO_2 into the ASMA. In Sect. 4, we provide a discussion exploring the effects of partitioning into the clouds and wet scavenging processes on the deep convective transport of NH_3 and SO_2 into the ASMA. A summary of the main findings and conclusions is given in Sect. 5.

2 Model description and setup

The EMAC model is a global atmospheric chemistry and climate model that combines the 5th generation European Centre – Hamburg general circulation model (ECHAM5) (Roeckner et al., 2006) with the Modular Earth Submodel System (MESSy) Atmospheric Chemistry system (Jöckel et al., 2006;Jöckel et al., 2010) to simulate atmospheric processes from the troposphere to the middle atmosphere and their interactions with oceans, land, and anthropogenic influences. For this study, we used the EMAC (ECHAM5 version 5.3.02, MESSy version 2.55.0), which includes the MESSy submodels describing various chemical, physical and dynamical processes in detail (Jöckel et al., 2016). The model resolution used in this study is T63L90, corresponding to a horizontal grid resolution of about $1.875^\circ \times 1.875^\circ$ and 90 vertical layers extending from the Earth's surface to an altitude of 0.01 hPa (~80 km).

In EMAC, heterogeneous and gas-phase chemistry are simulated online using the MECCA submodel (Sander et al., 2011;Sander et al., 2019). MECCA calculates the concentration of a range of gases and radicals, including reactive and aerosol precursor species, such as CO, SO_2, NH_3, nitrogen oxides ($NO_x \equiv NO + NO_2$), and volatile organic compounds (VOCs), and major oxidant species like OH, O_3, H_2O_2, and NO_3. In this study, the Mainz isoprene mechanism (Taraborrelli et al., 2009), and halogen and sulfur stratospheric chemistry (Brühl et al., 2015), were included in the MECCA calculation, following our previous work (Ma et al., 2019). Photolysis rates for the troposphere up to the mesosphere are calculated by the JVAL submodel (Jöckel et al., 2006), which considers absorption and scattering by gases, aerosols and clouds using a delta-two-stream method. The uptake of SO_2 and NH_3 and the aqueous-phase oxidation of SO_2 by H_2O_2 and O_3 in cloud droplets are calculated by the SCAV submodel (Tost et al., 2006a;Tost et al., 2007). The removal of gases and aerosols through wet deposition is calculated by the SCAV submodel (Tost et al., 2006a), and dry deposition is calculated by the DRYDEP submodel (Kerkweg et al., 2006).

Aerosol microphysics and gas/aerosol partitioning are treated by the GMXe submodel (Pringle et al., 2010), which uses seven interacting lognormal modes (M7) to describe the typical size range of aerosol species, including the nucleation mode and hydrophilic and hydrophobic Aitken, accumulation and coarse modes. The properties of aerosols in each mode are represented by the number concentration, total mass (internal mixture of contributing species), density, median radius, and width of the lognormal distribution. The inorganic aerosol composition is simulated by the ISORROPIA-II thermodynamic equilibrium model (Fountoukis and Nenes, 2007), with updates as discussed in the work of Capps et al. (2012).

Convective cloud processes and convective tracer transport are calculated using the CONVECT and CVTRANS submodels (Tost et al., 2006b), respectively. CONVECT consists of an interface for selecting different convection schemes (Tost et al.,

2006b), and in this study we used the Tiedtke convection scheme with Nordeng closure (Tiedtke, 1989;Nordeng, 1994), which has proven to be the best-performing, including in the recent work of Xenofontos et al. (2025). Convective cloud microphysics is based on temperature and moisture profiles, though without interactively accounting for the influence of aerosols on liquid droplet or ice formation processes. Large-scale cloud processes are described by the CLOUD submodel (Roeckner et al., 2006), and the original ECHAM5 cloud scheme without aerosol–cloud interactions was used for this study.

The CAMS-GLOB-ANT emission inventory (v4.2, https://eccad.sedoo.fr, last access: 1 November 2025), with a horizontal grid resolution of 0.5 °×0.5 °at monthly intervals, was utilized for surface anthropogenic emissions of the trace gases (including CO, NH_3 and SO_2) and aerosols in this study. For aircraft emissions, the CAMS-GLOB-AIR emission inventory (v1.1, https://eccad.sedoo.fr, last access: 1 November 2025) was used. The land and water biological emissions of NH_3 and non-methane hydrocarbons (NMHCs) are based on the Global Emissions Inventory Activity (GEIA) database (Bouwman et al., 1997). NO_x produced by lightning is calculated online and distributed vertically based on the parameterization of Price and Rind (1992). The NO soil emissions are calculated online according to the algorithm of Yienger and Levy II (1995). Biomass burning emissions are calculated by the BIOBURN submodel (Kaiser et al., 2012), which determines the fluxes based on biomass burning emission factors and dry matter combustion rates from the Global Fire Assimilation System (GFAS).

The SO_2 emissions from explosive volcanic eruptions occurring at different locations and latitudes were taken into account using the volcanic SO_2 plumes detected by various (occultation and limb-based) satellite instruments (Schallock et al., 2023). There were about 146 explosive volcanic eruption events accounted for the years 2010-2020, and a three-dimensional volcanic SO_2 plume (in unit of volume mixing ratio) for each event was added on-line to the background values of SO_2 in the UTLS at the corresponding time during the model simulation, as done in our previous work (Brühl et al., 2018;Ma et al., 2019).

The EMAC model has been evaluated against various observations of trace gases and aerosols in both the troposphere and stratosphere, including aircraft measurements conducted within the ASMA in some specific years (Gottschaldt et al., 2017;Lelieveld et al., 2018;Tomsche et al., 2019;Johansson et al., 2020;Xenofontos et al., 2024). These comparisons indicate that EMAC can simulate complex dynamic, physical and chemical processes from the PBL to the UTLS over the Asian summer monsoon region (e.g., Gottschaldt et al., 2018;Ma et al., 2019;Rosanka et al., 2021;Becker et al., 2025). In this study, the model simulation was performed for the years 2010–2020 at an integration time step of 10 minutes. The simulation was nudged by the ECMWF's ERA5 meteorological re-analysis data at time intervals of 6 hours (Hersbach et al., 2020). The nudging was exerted for temperature, vorticity, divergence, and surface pressure, with maximum weights at the model levels from about 10 hPa to 706 hPa (except for surface pressure). The chemical initial conditions of trace gases and aerosols were provided by the results of a previous simulation using EMAC T106L90 (Ma et al., 2019). The simulation results were output at 5-hour intervals for analysis.

3 Results

The objective of this study is to investigate the deep convective transport of the primary gaseous pollutants CO, NH_3 and SO_2 from the planetary boundary layer (PBL) to the Asian summer monsoon anticyclone (ASMA). During the summer season, i.e.,

June-August (JJA), deep convection associated with the Asian summer monsoon is observed each year (Houze Jr. et al., 2015) and is selected for the analysis. We focus on the climatology of deep convective transport of selected trace gases into the ASMA in JJA during 2010-2020.

3.1 Spatial distributions of CO, NH₃ and SO₂ in the PBL during the Asian summer monsoon

5   The Asian summer monsoon region is characterized by enhanced precipitation, strong and deep convection, and a distinct vertical structure in the circulation, with a cyclonic flow and convergence in the lower troposphere and a strong anticyclone and divergence in the UTLS (Krishnamurti and Bhalme, 1976;Hoskins and Rodwell, 1995;Wang and LinHo, 2002). These climatic features associated with the Asian summer monsoon are well captured by our EMAC model with 11 years of simulated meteorological data (see Fig. S1). Figure 1 shows the averaged PBL's wind field and volume mixing ratios of CO, NH₃ and

10 SO₂ in JJA over the years 2010-2020. The influence and footprints of the large anthropogenic emission sources near the Earth's surface, especially those in northern India and eastern China (see Fig. S2), are clearly evident in the geographic distributions of these primary gaseous pollutants within the PBL. As shown in Fig. 1, in the PBL, the pollutants from South Asia (northern India in particular) can be transported by the cyclonic flow (dominated by southwesterlies over the Indian subcontinent) to the southern flank of the Tibetan Plateau. Further transport of these pollutants to the large Tibetan Plateau platform appears to be

15 limited by the topographical block at the steep southern slopes of the plateau with less thermal impact (Boos and Kuang, 2010).

While the PBL's CO levels are comparable between northern India and eastern China, the PBL's NH₃ levels are 5-10 ppbv higher in northern India than in eastern China and, in contrast, the PBL's SO₂ levels are 4-8 ppbv lower in northern India than in eastern China (Fig. 1). For NH₃, IASI satellite observations also showed a similar spatial distribution pattern, with higher abundance over northern India than eastern China, due to stronger emission strength from the former (Liu et al., 2022;Luo et

20 al., 2022). As can be estimated from Fig. 1, the ratios of the PBL's NH₃ volume mixing ratio to the PBL's SO₂ volume mixing ratio are about 4-6 in northern India, and these ratios drop to 1.5-2 in eastern China. Since NH₃ is an alkaline gas and SO₂ is an acidic gas, changes in their relative abundance will affect aqueous-phase chemistry and the scavenging process when they are dissolved in clouds (Seinfeld and Pandis, 2006).

3.2 Deep convection frequency and spatial distributions of CO, NH₃ and SO₂ within the ASMA

25 Deep convection usually occurs as part of a mesoscale convective system with a sufficient moisture supply at cloud base (Houze Jr., 2004). Strong ascent with deep convection can reach the upper troposphere above 10 km above sea level (a.s.l., hereafter, all altitudes are referred to a.s.l. unless specified otherwise), and even higher into the lower stratosphere (Meenu et al., 2010;Emmanuel et al., 2021). The ASMA is located at an altitude range of about 10 km to 18 km in the vertical, and horizontally it covers a larger area ranging 30-120°E and 20-40°E, which can be highlighted using the geopotential height

30 distribution at 100 mPa (Fig. S1) as done by Basha et al. (2020). For this study, we used the convective cloud top heights output at intervals of 5 hours over the simulation period to count the events of deep convection reaching a selected altitude

(e.g., 10 km) or higher. Then, we calculated the frequency of deep convection at the defined altitudes by dividing the number of deep convection events by the total number across all datasets (including both cloudy and cloud-free cases) used for counting.

Figure 2 presents the deep convection frequency for JJA during 2010-2020 for the convective cloud top heights above 10 km, 12 km, 14km, and 16 km, respectively, corresponding to the main vertical range of the ASMA. Except for the oceanic regions, the frequency of deep convection reaching altitudes above 10 km is the highest (up to ~20%) over the Tibetan Plateau among the continental Asian summer monsoon regions. Even at altitudes above 14 km, the frequency of deep convection is prominently high (up to 10%) over the Tibetan Plateau compared to the surrounding regions within the ASMA. It is also shown that deep convection can reach to altitudes above 16 km over the Tibetan Plateau, although the corresponding frequencies are as small as ~1% or less, lower than those over the surrounding areas to its south within the ASMA. These results are in agreement with previous studies in that convective clouds form frequently over the Tibetan Plateau due to the abundant water vapor convergence, elevated land surface and strong radiative heating (e.g., Sugimoto and Ueno, 2010;Xu et al., 2014). They are also consistent with the work of Legras and Bucci (2020), which shows that the Tibetan Plateau, with the largest number of high clouds, favours the deep convective transport of compounds released from ground level to much higher altitudes, even into the lower stratosphere.

Figure 3 shows the averaged volume mixing ratios of CO, NH_3 and SO_2 at the selected altitudes of 10-12 km and 14-16 km in JJA over the years 2010-2020, respectively. It can be seen that the spatial distributions of CO, NH_3, and SO_2 within the ASMA differ. The enhancements of CO and NH_3 within the ASMA are clearly visible, with the maxima occurring over northern India and the southern edge of the Tibetan Plateau for CO and over the southern and eastern parts of the Tibetan Plateau for NH_3. The CO spatial distribution character within the ASMA, as simulated in this study, has been well recognized by a large number of previous studies (e.g., Park et al., 2007;Santee et al., 2017). The NH_3 enhancements within the ASMA characterized by this study are also in agreement with the satellite observations and model study before (Höpfner et al., 2016;Ge et al., 2018;Ma et al., 2019).

An analysis of the MIPAS satellite data showed the enhanced mixing ratios of SO_2 at altitudes of 16-18 km within the ASMA (Höpfner et al., 2015), but these enhancements of SO_2 are not as significant as those of CO and NH_3. Figure 3 indicates that SO_2 enhancements occur over central India (a small area around 20 °N latitude) and eastern China, but these enhancements are very weak. In contrast, our simulation shows a decrease of SO_2 over the southern Tibetan Plateau relative to the surroundings within the ASMA, which was not detected by satellite measurements. According to our simulation, SO_2 levels within the ASMA are very low (below 0.05 ppbv), similar to those reported by Höpfner et al. (2015). For SO_2, the averaged mixing ratios in the upper troposphere within the ASMA are about two orders of magnitude lower than those in the polluted area within the PBL, whereas they are about one order of magnitude lower for NH_3 and only a few times lower for CO.

3.3 Tendency and efficiency of the deep convective transport of CO, NH₃ and SO₂ into the ASMA

As mentioned in Sect. 2, convective transport of the tracers was simulated using the CVTRANS submodel, with the updraft and downdraft mass fluxes, entrainment and detrainment calculated by the CONVECT submodel. In the CVTRANS scheme,

convective transport is calculated separately from scavenging, and the tracers are redistributed vertically without a net gain or loss in the whole convective column. The tendency of a tracer due to convective transport alone can be obtained from the difference in the tracer's mixing ratio before and after the implementation of CVTRANS. Here, in this study, the mean tendency is calculated by averaging the data across all time intervals, rather than only for deep convection events.

5   Figure 4 shows the averaged deep convective transport tendency of CO, NH_3 and SO_2 at the selected altitudes of 10-12 km and 14-16 km in JJA over the years 2010-2020, respectively. Strong deep convective transport tendency within the ASMA can be found over northern India and the southern edge of the Tibetan Plateau for CO (0.2-0.5 ppbv hr^{-1}), over the southern and eastern parts of the Tibetan Plateau for NH_3 (0.02-0.05 ppbv hr^{-1}), and over central India and eastern China for SO_2 (0.002-0.005 ppbv hr^{-1}). These spatial distribution patterns in the deep convective transport tendency are similar to those in the volume

10   mixing ratios of CO, NH_3 and SO_2 shown in Fig. 3, indicating a dominant role of deep convection in the enhancements of CO, NH_3 and SO_2 within the ASMA. It can be seen that the maximum tendency for SO_2 (e.g., over central India) is much lower (by an order of magnitude) than that for NH_3 (e.g., over the southern Tibetan Plateau). Moreover, in contrast to CO and NH_3, an enhancement of the strong deep convective transport tendency cannot be found for SO_2 over the southern Tibetan Plateau. It is indicated that, in addition to the deep convective transport itself, other factors, e.g., the scavenging process associated with

15   it, influence the amount of pollutants reaching the ASMA.

In this study, the deep convective transport efficiency of a trace gas into the ASMA is defined by the ratio of the updraft mass flux of this trace gas at a selected height (i.e., 10 km) to its maximum near the cloud base in the convective column (see Fig. S3). The updraft mass flux of a trace gas is calculated as the updraft mass flux of the air times the mass mixing ratio of this trace gas at the same altitude. It can be expected that, in addition to convective activity, cloud scavenging may influence

20   the deep convective transport efficiency of the trace gas by reducing the amount that reaches the ASMA.

Figure 5 shows the mean deep convective transport efficiency of CO, NH_3 and SO_2 into the ASMA (defined with a lower boundary of 10 km height) in JJA over the years 2010-2020, respectively. The deep convective transport efficiency is very high (above 50%) over the central and southern Tibetan Plateau for all three trace gases considered, indicating that the middle troposphere of the Tibetan Plateau is an effective pathway for transporting pollutants from the PBL to the ASMA. With a low

25   solubility and thus not affected by scavenging, CO has a higher deep convective transport efficiency than NH_3 and SO_2 over all the continental regions where deep convection occurs. For instance, over the southern Tibetan Plateau, the maximum in the deep convective transport efficiency reaches about 80%-90% for CO, 60%-70% for NH_3, and 60%-80% for SO_2. Over northern India (excluding the southern flank of the Tibetan Plateau), the deep convective transport efficiency is 20%-30% for CO, 2%-4% for NH_3, and less than 1% for SO_2. The deep convective transport efficiency of SO_2 calculated here appears to be

30   comparable to that of NH_3 over the southern Tibetan Plateau It should be noted that there could be an overestimation of the deep convective transport efficiency of SO_2 here since a considerable fraction of SO_2 in the upper troposphere might come from other sources than Asian surface emissions, e.g., volcanic SO_2 from explosive eruptions (Neely et al., 2014;Ma et al., 2019).

4 Discussion

In this section, we aim to explain the results presented in the above section (Sect. 3) by investigating the cloud and wet scavenging processes over the Asian summer monsoon region during the same period (i.e., JJA during 2010-2020). Among the three trace gases, only the cloud and wet scavenging processes of NH_3 and SO_2 are investigated since CO has a low

5 solubility and is not considered in the EMAC submodel SCAV. The focus is on the causes of the difference between NH_3 and SO_2 in the deep convective transport from the PBL to the ASMA.

4.1 Partitioning of NH₃ and SO₂ between the gas and liquid phases in clouds

In the above section, we show that the middle troposphere over the Tibetan Plateau is an effective pathway of transporting the pollutants from the PBL to the ASMA by deep convection, with some differences in the deep convective transport efficiency

10 for different trace gases, e.g., CO vs. NH_3, and NH_3 vs. SO_2 (Fig. 5). To investigate the effect of cloud process on the differences, we looked at the vertical column densities of gaseous NH_3 and SO_2 in the air (denoted as NH_3(air) and SO_2(air), simply as NH_3 and SO_2), their dissolving and reaction products in the clouds (denoted as NHx(liq) and SOx(liq)), and the total (i.e., NH_3(air)+NHx(liq) and SO_2(air)+SOx(liq)) within a height range of 6-10 km for the simulation period (see Fig. S4). The NHx in the clouds is the sum of liquid ammonia and ammonium, i.e., NHx(liq) $\equiv$ NH_3(liq) + NH_4^+(liq). The SOx in the clouds is

15 the sum of liquid SO_2 and its dissociation and oxidation products (denoted by S(IV) and S(VI)), i.e., SOx(liq) $\equiv$ S(IV, liq) + S(VI, liq), where S(IV, liq) $\equiv$ SO_2(liq) + HSO_3^-(liq) + SO_3^{2-}(liq) and S(VI, liq) $\equiv$ H_2SO_4(liq) + HSO_4^-(liq) + SO_4^{2-}(liq). It is noted that for the investigated region and period of this study, NHx(liq) and SOx(liq) are dominated by NH_4^+(liq) (>99.9%) and SO_4^{2-}(liq) plus HSO_4^-(liq) (>99%), respectively.

Figure 6 shows the relative contributions of the liquid NHx and SOx in the clouds to the total (gas-phase plus liquid-phase)

20 within a vertical column of 6-10 km in JJA during 2010-2020, respectively. One can see considerable amounts of gaseous NH_3 and SO_2 at heights above 6 km over the Tibetan Plateau partitioning into the clouds before reaching the ASMA. Similar to the spatial distributions of NH_3 and SO_2, the enhancements in the 6-10 km vertical columns of cloudy NHx(liq) and SOx(liq) occur over the Tibetan Plateau as well (Fig. 4S). The relative contributions of the 6-10 km column in the clouds to the total (gas-phase plus liquid-phase) over the Tibetan Plateau are about 10-30% for NHx(liq) and 50-80% for SOx(liq), respectively. In

25 this study, the primary partitioning of the soluble gases between the gas and liquid phases was treated with Henry's law, with a Henry's law constant of 203 M atm^{-1} for NH_3 and 3.13 M atm^{-1} for SO_2 at a temperature of 0 ℃, respectively. While the environmental conditions, including the cloud liquid water content, are the same, the lower Henry's law constant for SO_2 than for NH_3 cannot explain the higher fraction of SO_2 than NH_3 partitioning into the liquid phase simulated by the model. The gases dissolved in water can dissociate into ions, e.g., NH_4^+(liq), HSO_3^-(liq), and SO_3^{2-}(liq), following chemical equilibria

30 included in the SCAV submodel. Therefore, the effective Henry's law coefficients, which consider trace gas dissociating into ions, are better to represent the partitioning of the trace gases like NH_3 between the gas and liquid phases (Seinfeld and Pandis, 2006). Under atmospheric conditions, practically all dissolved ammonia in clouds exists as the ammonium ion. Moreover, in

the clouds the concentration level of S(VI, liq) is two orders of magnitude higher than that of S(IV, liq) according to our simulation (not shown). This indicates that the oxidation of S(IV, liq) to S(VI, liq) is an important factor influencing the partitioning of SO_2 between the gas and liquid phases, and it can result in higher fractions of SO_2 than NH_3 partitioning into the liquid phase, as shown in Fig. 6.

5   4.2 Wet removal of NH_3 and SO_2 through aqueous NH_4^+ and S(VI) in the ASM region

Being very soluble and reactive in water, NH_3 and SO_2 partitioned into the cloud droplets can be efficiently removed from the atmosphere by wet deposition of their aqueous reaction products NHx(liq) and SOx(liq). As for NHx(liq) and SOx(liq) in the clouds mentioned above (Sect. 4.1), NHx(liq) and SOx(liq) in rain are also mainly (>99%) in the form of NH_4^+(liq) and SO_4^{2-}(liq) plus HSO_4^-(liq), respectively. Figure 7 shows the wet deposition fluxes of NHx(liq) and SOx(liq) averaged for JJA over

10   the years 2010-2020, respectively. Strong wet deposition fluxes of NHx(liq) and SOx(liq) occur in the polluted regions, such as northern India and eastern China, corresponding to the large emission rates of NH_3 and SO_2 there (Fig. S2). They are also affected by the precipitation rate and spatial distribution (Fig. S1c). For example, the simulated SOx(liq) wet deposition fluxes are negligible in Saudi Arabia due to extremely low precipitation, although the SO_2 emissions are large in some areas there. The maximum wet deposition fluxes of both NHx(liq) and SOx(liq) are found on the southern and eastern slopes of the Tibetan

15   Plateau, corresponding to the highest precipitation rates there.

Numerical studies have highlighted the very strong precipitation occurring along the southern slopes of the Tibetan Plateau and its role in the monsoon circulation (e.g., Bao and Li, 2020). This precipitation removes aerosols over the Tibetan Plateau by wet scavenging (Liu et al., 2023). Our model results indicate that in addition to the topographical block, the removal by wet scavenging along the southern slopes is very effective at reducing the amounts of NH_3 and SO_2 reaching the Tibetan Plateau

20   (Fig. 1 and Fig. 7). Such scavenging is more effective for SO_2 than NH_3, resulting much lower amounts of SO_2 available for the deep convective transport from the lower troposphere of the Tibetan Plateau to the ASMA. While the deep convection frequency (shown in Fig. 2) is a dominant factor, the concentration levels of the tracers in the PBL (shown in Fig. 1) and scavenging efficiency are also important for determining the amount of the tracers transported into the ASMA (Fig. 4). This can explain the causes of the minima in both the deep convective transport tendency and volume mixing ratio of SO_2 within

25   the ASMA occurring over the southern Tibetan Plateau.

We quantify the effectiveness of precipitation in removing NH_3 and SO_2 by comparing their atmospheric lifetimes with wet deposition, calculated as the tropospheric vertical column density (below 10 km) divided by the wet deposition flux for each trace gas. Figure 8 shows the mean atmospheric lifetime of tropospheric NH_3 and SO_2 against wet deposition in JJA during 2010-2020. It can be seen that over the southern parts and slopes of the Tibetan Plateau, the lifetime against wet

30   deposition is around 1-2 days for NH_3 and less than 1 day for SO_2, respectively. The lifetime of SO_2 is shorter than that of NH_3 against wet deposition over northern India, the Tibetan Plateau and its southern slopes, and vice versa over eastern China. Such a turnaround could be due to differences in the relative amounts of tropospheric SO_2 and NH_3 over these regions. The ratio of the tropospheric vertical column density of NH_3 to that of SO_2 appears to be much larger over northern India than over eastern

China (see Fig. S5). The NH_3 column over northern India is the largest over the globe as reported in a previous study (Wang et al., 2020). It should be noted that NH_3 and SO_2 are alkaline and acidic gases, tending to neutralize each other to form $NH_4^+(liq)$ and $SO_4^{2-}(liq)$ or $HSO_4^-(liq)$ in the clouds, respectively. The large and excess amounts of NH_3 relative to SO_2 over northern India not only favour the deep convective transport of more NH_3 from the PBL to the ASMA, but also limit the amounts of SO_2 transported to the Tibetan Plateau by enhancing its partitioning into the clouds and removal by wet deposition.

5 Conclusions

We have investigated the deep convective transport of trace gases CO, NH_3 and SO_2 from the planetary boundary layer (PBL) to the Asian summer monsoon anticyclone (ASMA) using the global atmospheric chemistry and climate model EMAC at T63L90 resolution. The model simulation was performed for the period from January 2010 to December 2020, and for this study 11 years of the seasonally averaged results for June–August (JJA) have been analyzed. The focus is on the similarities and differences in the transport efficiency of CO, NH_3, and SO_2 from the PBL, in particular from the South Asian PBL, to the ASMA.

By analysing the spatial distributions of convective cloud top height, we show that the frequency of deep convection reaching into the ASMA (defined as having a lower boundary at 10 km) is the highest (up to 20%) over the Tibetan Plateau among the continental Asian summer monsoon regions. Such a high deep convection frequency favours the efficient transport of trace gases from the lower troposphere of the Tibetan Plateau to the ASMA. Here for the first time, we quantify the deep convective transport efficiency of the trace gases CO, NH_3 and SO_2 into the ASMA by the ratio of the updraft mass flux of trace gas at the lower boundary of the ASMA (i.e., 10 km height) to its maximum near the convective cloud base. The results show that the deep convective transport efficiency is very high (above 50%) over the Tibetan Plateau for all three trace gases considered, with maximum values of about 80%-90% for CO, 60%-70% for NH_3, and 60%-80% for SO_2. Over the Indo-Gangetic plane, the deep convective transport efficiency is 20%-30% for CO, 2%-4% for NH_3, and less than 1% for SO_2.

Our model simulations show that the strongest deep convective transport tendency within the ASMA tends to occur over northern India and the southern edge of the Tibetan Plateau for CO (0.2-0.5 ppbv hr^{-1}), over the southern and eastern parts of the Tibetan Plateau for NH_3 (0.02-0.05 ppbv hr^{-1}), and over central India and eastern China for SO_2 (0.002-0.005 ppbv hr^{-1}). These spatial distribution patterns of deep convective transport tendency match well with those of the volume mixing ratios of CO, NH_3 and SO_2 within the ASMA, respectively. While the enhancements of CO and NH_3 within the ASMA are evident, the enhancements of SO_2 are very weak. In contrast to CO and NH_3, we find a decrease in SO_2 over the southern Tibetan Plateau relative to the surroundings within the ASMA.

We find considerable amounts of gaseous NH_3 and SO_2 at heights above 6 km over the Tibetan Plateau partitioning into the clouds before reaching the ASMA, with the relative contributions of the 6-10 km column in the clouds (liquid-phase) to the total (gas-phase plus liquid-phase) of about 10-30% for NH_3 (in the form of $NH_4^+(liq)$) and 50-80% for SO_2 (mainly in the form of $SO_4^{2-}(liq)$ and $HSO_4^-(liq)$), respectively. Our model simulations show that the removal by wet deposition on the southern slopes plays an important role in reducing the amounts of NH_3 and SO_2 reaching the Tibetan Plateau platform. Such

scavenging is more effective for SO_2 than for NH_3, with lifetimes of 1-2 days for NH_3 and less than 1 day for SO_2. We argue that the large and excess amounts of NH_3 relative to SO_2 over northern India not only favour the deep convective transport of more NH_3 from the PBL to the ASMA, but also limit the amounts of SO_2 transported to the Tibetan Plateau and then the ASMA by enhancing its partitioning into the clouds and removal by wet deposition. Moreover, deep convection is generally accompanied by lightning activity, which can release NO_x and further produce HNO_3 through oxidation reactions. While NH_3 is alkaline, SO_2 and HNO_3 are acidic gases, and they are all gaseous precursors of aerosols in the ATAL Ongoing changes in emissions of NH_3, SO_2 and NO_x and their interactions through multi-phase chemistry during deep convective transport may have significant impacts on the chemical characteristics of ASMA, which require continued investigation.

Supplement. The supplement related to this article is available online.

Author contributions. JM, QH and JL initiated the project. JM performed the model simulations and analyzed the data. BC, QH, XY, GW, and SC contributed to the data analysis. BS, CB, AP, and JL contributed to the model simulation. JM prepared the manuscript with contributions from all co-authors.

Competing interests. At least one of the (co-)authors is a member of the editorial board of Atmospheric Chemistry and Physics. The authors have no other competing interests to declare.

Special issue statement. This article is part of the special issue "The Modular Earth Submodel System (MESSy) (ACP/GMD inter-journal SI)". It is not associated with a conference.

References

Appel, O., Köllner, F., Dragoneas, A., Hünig, A., Molleker, S., Schlager, H., Mahnke, C., Weigel, R., Port, M., Schulz, C., Drewnick, F., Vogel, B., Stroh, F., and Borrmann, S.: Chemical analysis of the Asian tropopause aerosol layer (ATAL) with emphasis on secondary aerosol particles using aircraft-based in situ aerosol mass spectrometry, Atmos. Chem. Phys., 22, 13607-13630, 10.5194/acp-22-13607-2022, 2022.

Bao, Q., and Li, J.: Progress in climate modeling of precipitation over the Tibetan Plateau, National Science Review, 7, 486-487, 10.1093/nsr/nwaa006, 2020.

Barth, M. C., Kim, S.-W., Skamarock, W. C., Stuart, A. L., Pickering, K. E., and Ott, L. E.: Simulations of the redistribution of formaldehyde, formic acid, and peroxides in the 10 July 1996 Stratospheric-Tropospheric Experiment: Radiation, Aerosols, and Ozone deep convection storm, Journal of Geophysical Research: Atmospheres, 112, https://doi.org/10.1029/2006JD008046, 2007.

Barth, M. C., Lee, J., Hodzic, A., Pfister, G., Skamarock, W. C., Worden, J., Wong, J., and Noone, D.: Thunderstorms and upper troposphere chemistry during the early stages of the 2006 North American Monsoon, Atmos. Chem. Phys., 12, 11003-11026, 10.5194/acp-12-11003-2012, 2012.

Barth, M. C., Cantrell, C. A., Brune, W. H., Rutledge, S. A., Crawford, J. H., Huntrieser, H., Carey, L. D., MacGorman, D., Weisman, M., Pickering, K. E., Bruning, E., Anderson, B., Apel, E., Biggerstaff, M., Campos, T., Campuzano-Jost, P., Cohen, R., Crounse, J., Day, D. A., Diskin, G., Flocke, F., Fried, A., Garland, C., Heikes, B., Honomichl, S., Hornbrook, R., Huey, L. G., Jimenez, J. L., Lang, T., Lichtenstern, M., Mikoviny, T., Nault, B., O'Sullivan, D., Pan, L. L., Peischl, J., Pollack, I., Richter, D., Riemer, D., Ryerson, T., Schlager, H., Clair, J. S., Walega, J., Weibring, P., Weinheimer, A., Wennberg, P., Wisthaler, A., Wooldridge, P. J., and Ziegler, C.: The Deep Convective Clouds and Chemistry (DC3) Field Campaign, Bulletin of the American Meteorological Society, 96, 1281-1309, 10.1175/bams-d-13-00290.1, 2015.

Basha, G., Ratnam, M. V., and Kishore, P.: Asian summer monsoon anticyclone: trends and variability, Atmos. Chem. Phys., 20, 6789-6801, 10.5194/acp-20-6789-2020, 2020.

Becker, F., Vogel, B., Günther, G., Ploeger, F., Riese, M., Rosanka, S., Taraborrelli, D., Nützel, M., Jöckel, P., Brinkop, S., and Müller, R.: Upward transport of boundary layer air to altitudes of the Asian summer monsoon anticyclone in Eulerian and Lagrangian model simulations, Meteorologische Zeitschrift, 10.1127/metz/1266, 2025.

Bela, M. M., Barth, M. C., Toon, O. B., Fried, A., Homeyer, C. R., Morrison, H., Cummings, K. A., Li, Y., Pickering, K. E., Allen, D. J., Yang, Q., Wennberg, P. O., Crounse, J. D., St. Clair, J. M., Teng, A. P., O'Sullivan, D., Huey, L. G., Chen, D., Liu, X., Blake, D. R., Blake, N. J., Apel, E. C., Hornbrook, R. S., Flocke, F., Campos, T., and Diskin, G.: Wet

scavenging of soluble gases in DC3 deep convective storms using WRF-Chem simulations and aircraft observations, Journal of Geophysical Research: Atmospheres, 121, 4233-4257, https://doi.org/10.1002/2015JD024623, 2016.

Bergman, J. W., Fierli, F., Jensen, E. J., Honomichl, S., and Pan, L. L.: Boundary layer sources for the Asian anticyclone: Regional contributions to a vertical conduit, Journal of Geophysical Research: Atmospheres, 118, 2560-2575, 10.1002/jgrd.50142, 2013.

Bertram, T. H., Perring, A. E., Wooldridge, P. J., Crounse, J. D., Kwan, A. J., Wennberg, P. O., Scheuer, E., Dibb, J., Avery, M., Sachse, G., Vay, S. A., Crawford, J. H., McNaughton, C. S., Clarke, A., Pickering, K. E., Fuelberg, H., Huey, G., Blake, D. R., Singh, H. B., Hall, S. R., Shetter, R. E., Fried, A., Heikes, B. G., and Cohen, R. C.: Direct Measurements of the Convective Recycling of the Upper Troposphere, Science, 315, 816-820, 10.1126/science.1134548, 2007.

Bian, J., Li, D., Bai, Z., Li, Q., Lyu, D., and Zhou, X.: Transport of Asian surface pollutants to the global stratosphere from the Tibetan Plateau region during the Asian summer monsoon, National Science Review, 10.1093/nsr/nwaa005, 2020.

Boos, W. R., and Kuang, Z.: Dominant control of the South Asian monsoon by orographic insulation versus plateau heating, Nature, 463, 218-222, 10.1038/nature08707, 2010.

Bouwman, A. F., Lee, D. S., Asman, W. A. H., Dentener, F. J., Van Der Hoek, K. W., and Olivier, J. G. J.: A global high-resolution emission inventory for ammonia, Global Biogeochemical Cycles, 11, 561-587, doi:10.1029/97GB02266, 1997.

Brühl, C., Lelieveld, J., Tost, H., Höpfner, M., and Glatthor, N.: Stratospheric sulfur and its implications for radiative forcing simulated by the chemistry climate model EMAC, Journal of Geophysical Research: Atmospheres, 120, 2103-2118, 10.1002/2014JD022430, 2015.

Brühl, C., Schallock, J., Klingmüller, K., Robert, C., Bingen, C., Clarisse, L., Heckel, A., North, P., and Rieger, L.: Stratospheric aerosol radiative forcing simulated by the chemistry climate model EMAC using Aerosol CCI satellite data, Atmos. Chem. Phys., 18, 12845−12857, 10.5194/acp-18-12845-2018, 2018.

Capps, S. L., Henze, D. K., Hakami, A., Russell, A. G., and Nenes, A.: ANISORROPIA: the adjoint of the aerosol thermodynamic model ISORROPIA, Atmos. Chem. Phys., 12, 527-543, 10.5194/acp-12-527-2012, 2012.

Chatfield, R. B., and Crutzen, P. J.: Sulfur dioxide in remote oceanic air: Cloud transport of reactive precursors, Journal of Geophysical Research: Atmospheres, 89, 7111-7132, https://doi.org/10.1029/JD089iD05p07111, 1984.

Chen, B., Xu, X. D., Yang, S., and Zhao, T. L.: Climatological perspectives of air transport from atmospheric boundary layer to tropopause layer over Asian monsoon regions during boreal summer inferred from Lagrangian approach, Atmos. Chem. Phys., 12, 5827-5839, 10.5194/acp-12-5827-2012, 2012.

Chen, B., Ma, J., Zhang, W., Bian, J., Zhao, T., and Xu, X.: Recent Enhanced Deep Troposphere-to-Stratosphere Air Mass Transport Accompanying the Weakening Asian Monsoon, Journal of Meteorological Research, 38, 708-719, 10.1007/s13351-024-3155-5, 2024.

Dickerson, R. R., Huffman, G. J., Luke, W. T., Nunnermacker, L. J., Pickering, K. E., Leslie, A. C. D., Lindsey, C. G., Slinn, W. G. N., Kelly, T. J., Daum, P. H., Delany, A. C., Greenberg, J. P., Zimmerman, P. R., Boatman, J. F., Ray, J. D., and

Stedman, D. H.: Thunderstorms: An Important Mechanism in the Transport of Air Pollutants, Science, 235, 460-465, 10.1126/science.235.4787.460, 1987.

Ebert, M., Weigel, R., Weinbruch, S., Schneider, L., Kandler, K., Lauterbach, S., Köllner, F., Plöger, F., Günther, G., Vogel, B., and Borrmann, S.: Characterization of refractory aerosol particles collected in the tropical upper troposphere–lower stratosphere (UTLS) within the Asian tropopause aerosol layer (ATAL), Atmos. Chem. Phys., 24, 4771-4788, 10.5194/acp-24-4771-2024, 2024.

Emmanuel, M., Sunilkumar, S. V., Muhsin, M., Satheesh Chandran, P. R., Parameswaran, K., Kumar, B. S., Maitra, A., Satyanarayana, A. N. V., and Nagendra, N.: Effect of monsoon dynamics and deep convection on the upper troposphere lower stratosphere water vapour over Indian monsoon region, Atmospheric Research, 249, 105336, https://doi.org/10.1016/j.atmosres.2020.105336, 2021.

Fadnavis, S., Semeniuk, K., Pozzoli, L., Schultz, M. G., Ghude, S. D., Das, S., and Kakatkar, R.: Transport of aerosols into the UTLS and their impact on the Asian monsoon region as seen in a global model simulation, Atmos. Chem. Phys., 13, 8771-8786, 10.5194/acp-13-8771-2013, 2013.

Fadnavis, S., Sabin, T. P., Roy, C., Rowlinson, M., Rap, A., Vernier, J.-P., and Sioris, C. E.: Elevated aerosol layer over South Asia worsens the Indian droughts, Sci Rep-Uk, 9, 10268, 10.1038/s41598-019-46704-9, 2019.

Fountoukis, C., and Nenes, A.: ISORROPIA II: a computationally efficient thermodynamic equilibrium model for K^+ -Ca^{2+} -Mg^{2+} -NH_4^+ -Na^+ -SO_4^{2-} -NO_3^- -Cl^- -H_2O aerosols, Atmos. Chem. Phys., 7, 4639-4659, 10.5194/acp-7-4639-2007, 2007.

Fu, R., Hu, Y., Wright, J. S., Jiang, J. H., Dickinson, R. E., Chen, M., Filipiak, M., Read, W. G., Waters, J. W., and Wu, D. L.: Short circuit of water vapor and polluted air to the global stratosphere by convective transport over the Tibetan Plateau, Proceedings of the National Academy of Sciences, 103, 5664-5669, 10.1073/pnas.0601584103, 2006.

Ge, C., Zhu, C., Francisco, J. S., Zeng, X. C., and Wang, J.: A molecular perspective for global modeling of upper atmospheric NH_3 from freezing clouds, Proceedings of the National Academy of Sciences, 115, 6147-6152, 10.1073/pnas.1719949115, 2018.

Gottschaldt, K. D., Schlager, H., Baumann, R., Bozem, H., Eyring, V., Hoor, P., Jöckel, P., Jurkat, T., Voigt, C., Zahn, A., and Ziereis, H.: Trace gas composition in the Asian summer monsoon anticyclone: a case study based on aircraft observations and model simulations, Atmos. Chem. Phys., 17, 6091−6111, 10.5194/acp-17-6091-2017, 2017.

Gottschaldt, K. D., Schlager, H., Baumann, R., Cai, D. S., Eyring, V., Graf, P., Grewe, V., Jöckel, P., Jurkat-Witschas, T., Voigt, C., Zahn, A., and Ziereis, H.: Dynamics and composition of the Asian summer monsoon anticyclone, Atmos. Chem. Phys., 18, 5655−5675, 10.5194/acp-18-5655-2018, 2018.

Hanumanthu, S., Vogel, B., Müller, R., Brunamonti, S., Fadnavis, S., Li, D., Ölsner, P., Naja, M., Singh, B. B., Kumar, K. R., Sonbawne, S., Jauhiainen, H., Vömel, H., Luo, B., Jorge, T., Wienhold, F. G., Dirkson, R., and Peter, T.: Strong day-to-day variability of the Asian Tropopause Aerosol Layer (ATAL) in August 2016 at the Himalayan foothills, Atmos. Chem. Phys., 20, 14273-14302, 10.5194/acp-20-14273-2020, 2020.

He, Q., Ma, J., Zheng, X., Wang, Y., Wang, Y., Mu, H., Cheng, T., He, R., Huang, G., Liu, D., and Lelieveld, J.: Formation and dissipation dynamics of the Asian tropopause aerosol layer, Environmental Research Letters, 16, 014015, 10.1088/1748-9326/abcd5d, 2021.

Hersbach, H., Bell, B., Berrisford, P., Hirahara, S., Horányi, A., Muñoz-Sabater, J., Nicolas, J., Peubey, C., Radu, R., Schepers, D., Simmons, A., Soci, C., Abdalla, S., Abellan, X., Balsamo, G., Bechtold, P., Biavati, G., Bidlot, J., Bonavita, M., De Chiara, G., Dahlgren, P., Dee, D., Diamantakis, M., Dragani, R., Flemming, J., Forbes, R., Fuentes, M., Geer, A., Haimberger, L., Healy, S., Hogan, R. J., Hólm, E., Janisková, M., Keeley, S., Laloyaux, P., Lopez, P., Lupu, C., Radnoti, G., de Rosnay, P., Rozum, I., Vamborg, F., Villaume, S., and Thépaut, J.-N.: The ERA5 global reanalysis, Quarterly Journal of the Royal Meteorological Society, 146, 1999-2049, https://doi.org/10.1002/qj.3803, 2020.

Höpfner, M., Boone, C. D., Funke, B., Glatthor, N., Grabowski, U., Günther, A., Kellmann, S., Kiefer, M., Linden, A., Lossow, S., Pumphrey, H. C., Read, W. G., Roiger, A., Stiller, G., Schlager, H., von Clarmann, T., and Wissmüller, K.: Sulfur dioxide (SO2) from MIPAS in the upper troposphere and lower stratosphere 2002–2012, Atmos. Chem. Phys., 15, 7017-7037, 10.5194/acp-15-7017-2015, 2015.

Höpfner, M., Volkamer, R., Grabowski, U., Grutter, M., Orphal, J., Stiller, G., von Clarmann, T., and Wetzel, G.: First detection of ammonia (NH3) in the Asian summer monsoon upper troposphere, Atmos. Chem. Phys., 16, 14357-14369, 10.5194/acp-16-14357-2016, 2016.

Höpfner, M., Ungermann, J., Borrmann, S., Wagner, R., Spang, R., Riese, M., Stiller, G., Appel, O., Batenburg, A. M., Bucci, S., Cairo, F., Dragoneas, A., Friedl-Vallon, F., Hünig, A., Johansson, S., Krasauskas, L., Legras, B., Leisner, T., Mahnke, C., Möhler, O., Molleker, S., Müller, R., Neubert, T., Orphal, J., Preusse, P., Rex, M., Saathoff, H., Stroh, F., Weigel, R., and Wohltmann, I.: Ammonium nitrate particles formed in upper troposphere from ground ammonia sources during Asian monsoons, Nature Geoscience, 12, 608-612, 10.1038/s41561-019-0385-8, 2019.

Hoskins, B. J., and Rodwell, M. J.: A Model of the Asian Summer Monsoon. Part I: The Global Scale, Journal of the Atmospheric Sciences, 52, 1329-1340, 10.1175/1520-0469(1995)052<1329:amotas>2.0.co;2, 1995.

Hottmann, B., Hafermann, S., Tomsche, L., Marno, D., Martinez, M., Harder, H., Pozzer, A., Neumaier, M., Zahn, A., Bohn, B., Stratmann, G., Ziereis, H., Lelieveld, J., and Fischer, H.: Impact of the South Asian monsoon outflow on atmospheric hydroperoxides in the upper troposphere, Atmos. Chem. Phys., 20, 12655-12673, 10.5194/acp-20-12655-2020, 2020.

Houze Jr., R. A.: Mesoscale convective systems, Reviews of Geophysics, 42, https://doi.org/10.1029/2004RG000150, 2004.

Houze Jr., R. A., Rasmussen, K. L., Zuluaga, M. D., and Brodzik, S. R.: The variable nature of convection in the tropics and subtropics: A legacy of 16 years of the Tropical Rainfall Measuring Mission satellite, Reviews of Geophysics, 53, 994-1021, https://doi.org/10.1002/2015RG000488, 2015.

Iribarne, J. V., and Pyshnov, T.: The effect of freezing on the composition of supercooled droplets—I. Retention of HCl, HNO3, NH3 and H2O2, Atmospheric Environment. Part A. General Topics, 24, 383-387, https://doi.org/10.1016/0960-1686(90)90118-7, 1990.

Jöckel, P., Tost, H., Pozzer, A., Brühl, C., Buchholz, J., Ganzeveld, L., Hoor, P., Kerkweg, A., Lawrence, M., nbsp, G, Sander, R., Steil, B., Stiller, G., Tanarhte, M., Taraborrelli, D., van Aardenne, J., and Lelieveld, J.: The atmospheric chemistry general circulation model ECHAM5/MESSy1: consistent simulation of ozone from the surface to the mesosphere, Atmos. Chem. Phys., 6, 5067-5104, 10.5194/acp-6-5067-2006, 2006.

5   Jöckel, P., Kerkweg, A., Pozzer, A., Sander, R., Tost, H., Riede, H., Baumgaertner, A., Gromov, S., and Kern, B.: Development cycle 2 of the Modular Earth Submodel System (MESSy2), Geosci. Model Dev., 3, 717−752, 10.5194/gmd-3-717-2010, 2010.

Jöckel, P., Tost, H., Pozzer, A., Kunze, M., Kirner, O., Brenninkmeijer, C. A. M., Brinkop, S., Cai, D. S., Dyroff, C., Eckstein, J., Frank, F., Garny, H., Gottschaldt, K. D., Graf, P., Grewe, V., Kerkweg, A., Kern, B., Matthes, S., Mertens, M., Meul,
10   S., Neumaier, M., Nützel, M., Oberländer-Hayn, S., Ruhnke, R., Runde, T., Sander, R., Scharffe, D., and Zahn, A.: Earth System Chemistry integrated Modelling (ESCiMo) with the Modular Earth Submodel System (MESSy) version 2.51, Geosci. Model Dev., 9, 1153−1200, 10.5194/gmd-9-1153-2016, 2016.

Johansson, S., Höpfner, M., Kirner, O., Wohltmann, I., Bucci, S., Legras, B., Friedl-Vallon, F., Glatthor, N., Kretschmer, E., Ungermann, J., and Wetzel, G.: Pollution trace gas distributions and their transport in the Asian monsoon upper troposphere
15   and lowermost stratosphere during the StratoClim campaign 2017, Atmos. Chem. Phys., 20, 14695-14715, 10.5194/acp-20-14695-2020, 2020.

Johansson, S., Höpfner, M., Friedl-Vallon, F., Glatthor, N., Gulde, T., Huijnen, V., Kleinert, A., Kretschmer, E., Maucher, G., Neubert, T., Nordmeyer, H., Piesch, C., Preusse, P., Riese, M., Sinnhuber, B. M., Ungermann, J., Wetzel, G., and Woiwode, W.: Ammonia in the upper troposphere–lower stratosphere (UTLS): GLORIA airborne measurements for CAMS model
20   evaluation in the Asian monsoon and in biomass burning plumes above the South Atlantic, Atmos. Chem. Phys., 24, 8125-8138, 10.5194/acp-24-8125-2024, 2024.

Kachula, O., Vogel, B., Günther, G., and Müller, R.: An optimization-based approach to track the Asian summer monsoon anticyclone across daily and interannual variability, Atmos. Chem. Phys., 25, 15171-15195, 10.5194/acp-25-15171-2025, 2025.

25   Kaiser, J. W., Heil, A., Andreae, M. O., Benedetti, A., Chubarova, N., Jones, L., Morcrette, J. J., Razinger, M., Schultz, M. G., Suttie, M., and van der Werf, G. R.: Biomass burning emissions estimated with a global fire assimilation system based on observed fire radiative power, Biogeosciences, 9, 527-554, 10.5194/bg-9-527-2012, 2012.

Kar, J., Bremer, H., Drummond, J. R., Rochon, Y. J., Jones, D. B. A., Nichitiu, F., Zou, J., Liu, J., Gille, J. C., Edwards, D. P., Deeter, M. N., Francis, G., Ziskin, D., and Warner, J.: Evidence of vertical transport of carbon monoxide from
30   Measurements of Pollution in the Troposphere (MOPITT), Geophysical Research Letters, 31, L23105, 10.1029/2004gl021128, 2004.

Kerkweg, A., Buchholz, J., Ganzeveld, L., Pozzer, A., Tost, H., and Jöckel, P.: Technical Note: An implementation of the dry removal processes DRY DEPosition and SEDImentation in the Modular Earth Submodel System (MESSy), Atmos. Chem. Phys., 6, 4617-4632, 10.5194/acp-6-4617-2006, 2006.

17

Krishnamurti, T. N., and Bhalme, H. N.: Oscillations of a Monsoon System. Part I. Observational Aspects, Journal of the Atmospheric Sciences, 33, 1937-1954, 10.1175/1520-0469(1976)033<1937:ooamsp>2.0.co;2, 1976.

Krotkov, N. A., McLinden, C. A., Li, C., Lamsal, L. N., Celarier, E. A., Marchenko, S. V., Swartz, W. H., Bucsela, E. J., Joiner, J., Duncan, B. N., Boersma, K. F., Veefkind, J. P., Levelt, P. F., Fioletov, V. E., Dickerson, R. R., He, H., Lu, Z., and Streets, D. G.: Aura OMI observations of regional SO_2 and NO_2 pollution changes from 2005 to 2015, Atmos. Chem. Phys., 16, 4605-4629, 10.5194/acp-16-4605-2016, 2016.

Kunze, M., Braesicke, P., Langematz, U., and Stiller, G.: Interannual variability of the boreal summer tropical UTLS in observations and CCMVal-2 simulations, Atmos. Chem. Phys., 16, 8695-8714, 10.5194/acp-16-8695-2016, 2016.

Lee, K. O., Barret, B., Flochmoën, E. L., Tulet, P., Bucci, S., von Hobe, M., Kloss, C., Legras, B., Leriche, M., Sauvage, B., Ravegnani, F., and Ulanovsky, A.: Convective uplift of pollution from the Sichuan Basin into the Asian monsoon anticyclone during the StratoClim aircraft campaign, Atmos. Chem. Phys., 21, 3255-3274, 10.5194/acp-21-3255-2021, 2021.

Legras, B., and Bucci, S.: Confinement of air in the Asian monsoon anticyclone and pathways of convective air to the stratosphere during the summer season, Atmos. Chem. Phys., 20, 11045-11064, 10.5194/acp-20-11045-2020, 2020.

Lelieveld, J., and Crutzen, P. J.: Role of deep cloud convection in the ozone budget of the troposphere, Science, 264, 1759-1761, 1994.

Lelieveld, J., Bourtsoukidis, E., Brühl, C., Fischer, H., Fuchs, H., Harder, H., Hofzumahaus, A., Holland, F., Marno, D., Neumaier, M., Pozzer, A., Schlager, H., Williams, J., Zahn, A., and Ziereis, H.: The South Asian monsoon—pollution pump and purifier, Science, 361, 270-273, 10.1126/science.aar2501, 2018.

Li, D., Vogel, B., Müller, R., Bian, J., Günther, G., Ploeger, F., Li, Q., Zhang, J., Bai, Z., Vömel, H., and Riese, M.: Dehydration and low ozone in the tropopause layer over the Asian monsoon caused by tropical cyclones: Lagrangian transport calculations using ERA-Interim and ERA5 reanalysis data, Atmos. Chem. Phys., 20, 4133-4152, 10.5194/acp-20-4133-2020, 2020.

Li, D., Vogel, B., Müller, R., Bian, J. C., Günther, G., and Riese, M.: Tropical Cyclones Reduce Ozone in the Tropopause Region Over the Western Pacific: An Analysis of 18 Years Ozonesonde Profiles, Earths Future, 9, 10.1029/2020ef001635, 2021.

Li, D., Bian, J. C., Zhang, X., Vogel, B., Muller, R., and Gunther, G.: Impact of typhoon Soudelor on ozone and water vapor in the Asian monsoon anticyclone western Pacific mode, Atmospheric Science Letters, 24, 10.1002/asl.1147, 2023.

Li, Q., Jiang, J. H., Wu, D. L., Read, W. G., Livesey, N. J., Waters, J. W., Zhang, Y., Wang, B., Filipiak, M. J., Davis, C. P., Turquety, S., Wu, S., Park, R. J., Yantosca, R. M., and Jacob, D. J.: Convective outflow of South Asian pollution: A global CTM simulation compared with EOS MLS observations, Geophysical Research Letters, 32, L14826, 10.1029/2005gl022762, 2005.

Liu, P., Ding, J., Liu, L., Xu, W., and Liu, X.: Estimation of surface ammonia concentrations and emissions in China from the polar-orbiting Infrared Atmospheric Sounding Interferometer and the FY-4A Geostationary Interferometric Infrared Sounder, Atmos. Chem. Phys., 22, 9099-9110, 10.5194/acp-22-9099-2022, 2022.

Liu, W., Zhao, C., Xu, M., Feng, J., Du, Q., Gu, J., Leung, L. R., and Lau, W. K. M.: Southern Himalayas rainfall as a key
5   driver of interannual variation of pre-monsoon aerosols over the Tibetan Plateau, npj Climate and Atmospheric Science, 6, 57, 10.1038/s41612-023-00392-5, 2023.

Luo, Z., Zhang, Y., Chen, W., Van Damme, M., Coheur, P. F., and Clarisse, L.: Estimating global ammonia (NH3) emissions based on IASI observations from 2008 to 2018, Atmos. Chem. Phys., 22, 10375-10388, 10.5194/acp-22-10375-2022, 2022.

Ma, J., Brühl, C., He, Q., Steil, B., Karydis, V. A., Klingmüller, K., Tost, H., Chen, B., Jin, Y., Liu, N., Xu, X., Yan, P., Zhou,
10   X., Abdelrahman, K., Pozzer, A., and Lelieveld, J.: Modeling the aerosol chemical composition of the tropopause over the Tibetan Plateau during the Asian summer monsoon, Atmos. Chem. Phys., 19, 11587-11612, 10.5194/acp-19-11587-2019, 2019.

Ma, J., Zhou, X., Xu, X., Xu, X., Gromov, S., and Lelieveld, J.: Chapter 15 - Ozone and aerosols over the Tibetan Plateau, in: Asian Atmospheric Pollution, edited by: Singh, R. P., Elsevier, 287-302, 2022.

15   Meenu, S., Rajeev, K., Parameswaran, K., and Nair, A. K. M.: Regional distribution of deep clouds and cloud top altitudes over the Indian subcontinent and the surrounding oceans, Journal of Geophysical Research: Atmospheres, 115, https://doi.org/10.1029/2009JD011802, 2010.

Nützel, M., Brinkop, S., Dameris, M., Garny, H., Jöckel, P., Pan, L. L., and Park, M.: Climatology and variability of air mass transport from the boundary layer to the Asian monsoon anticyclone, Atmos. Chem. Phys., 22, 15659-15683, 10.5194/acp-
20   22-15659-2022, 2022.

Neely, R. R., Yu, P., Rosenlof, K. H., Toon, O. B., Daniel, J. S., Solomon, S., and Miller, H. L.: The contribution of anthropogenic SO$_2$ emissions to the Asian tropopause aerosol layer, Journal of Geophysical Research: Atmospheres, 119, 1571-1579, 10.1002/2013jd020578, 2014.

Nordeng, T. E.: Extended versions of the convection parametrization scheme at ECMWF and their impact on the mean and
25   transient activity of the model in the tropics, ECMWF Tech. Memo. 206, European Center for Medium-Range Weather Forecasts, Reading, UK, 1994.

Park, M., Randel, W. J., Gettelman, A., Massie, S. T., and Jiang, J. H.: Transport above the Asian summer monsoon anticyclone inferred from Aura Microwave Limb Sounder tracers, Journal of Geophysical Research: Atmospheres, 112, D16309, 10.1029/2006jd008294, 2007.

30   Park, M., Randel, W. J., Emmons, L. K., Bernath, P. F., Walker, K. A., and Boone, C. D.: Chemical isolation in the Asian monsoon anticyclone observed in Atmospheric Chemistry Experiment (ACE-FTS) data, Atmos. Chem. Phys., 8, 757-764, 2008.

Park, M., Randel, W. J., Emmons, L. K., and Livesey, N. J.: Transport pathways of carbon monoxide in the Asian summer monsoon diagnosed from Model of Ozone and Related Tracers (MOZART), Journal of Geophysical Research: Atmospheres, 114, D08303, 10.1029/2008jd010621, 2009.

Pickering, K. E., Thompson, A. M., Dickerson, R. R., Luke, W. T., McNamara, D. P., Greenberg, J. P., and Zimmerman, P. R.: Model calculations of tropospheric ozone production potential following observed convective events, J. Geophys. Res., 95, 1990.

Ploeger, F., Gottschling, C., Griessbach, S., Grooß, J. U., Guenther, G., Konopka, P., Müller, R., Riese, M., Stroh, F., Tao, M., Ungermann, J., Vogel, B., and von Hobe, M.: A potential vorticity-based determination of the transport barrier in the Asian summer monsoon anticyclone, Atmos. Chem. Phys., 15, 13145–13159, 10.5194/acp-15-13145-2015, 2015.

Ploeger, F., Konopka, P., Walker, K., and Riese, M.: Quantifying pollution transport from the Asian monsoon anticyclone into the lower stratosphere, Atmos. Chem. Phys., 17, 7055-7066, 10.5194/acp-17-7055-2017, 2017.

Price, C., and Rind, D.: A simple lightning parameterization for calculating global lightning distributions, Journal of Geophysical Research: Atmospheres, 97, 9919-9933, https://doi.org/10.1029/92JD00719, 1992.

Pringle, K. J., Tost, H., Message, S., Steil, B., Giannadaki, D., Nenes, A., Fountoukis, C., Stier, P., Vignati, E., and Lelieveld, J.: Description and evaluation of GMXe: a new aerosol submodel for global simulations (v1), Geosci. Model Dev., 3, 391–412, 10.5194/gmd-3-391-2010, 2010.

Pruppacher, H. R., and Klett, J.: Microphysics of Clouds and Precipitation, Kluwer Acad., Norwell, MA, 1997.

Randel, W. J., and Park, M.: Deep convective influence on the Asian summer monsoon anticyclone and associated tracer variability observed with Atmospheric Infrared Sounder (AIRS), Journal of Geophysical Research: Atmospheres, 111, D12314, 10.1029/2005jd006490, 2006.

Randel, W. J., Park, M., Emmons, L., Kinnison, D., Bernath, P., Walker, K. A., Boone, C., and Pumphrey, H.: Asian Monsoon Transport of Pollution to the Stratosphere, Science, 328, 611-613, 10.1126/science.1182274, 2010.

Ravindra Babu, S., Venkat Ratnam, M., Basha, G., Pani, S. K., and Lin, N. H.: Structure, dynamics, and trace gas variability within the Asian summer monsoon anticyclone in the extreme El Niño of 2015–2016, Atmos. Chem. Phys., 21, 5533-5547, 10.5194/acp-21-5533-2021, 2021.

Riese, M., Hoor, P., Rolf, C., Kunkel, D., Vogel, B., Köllner, F., Pöhlker, M., Ploeger, F., Ungermann, J., Woiwode, W., Johansson, S., Bauer, R., Barmpounis, K., Borrmann, S., Brauner, P., Clemens, J., Dragoneas, A., Ekinci, F., Emig, N., Engel, A., Eppers, O., Fadnavis, S., Friedl-Vallon, F., Geldenhuys, M., Günther, G., Grooß, J. U., Hegglin, M. I., Höpfner, M., Jesswein, M., Joppe, P., Kaumanns, J., Kachula, O., Keber, T., Kretschmer, E., Lachnitt, H. C., Lauther, V., Lloyd, P. E., Molleker, S., Müller, R., Neubert, T., Ort, L., Pöschl, U., Pöhlker, C., Rapp, M., Retzlaff, M., Rhode, S., Schneider, J., Schuck, T., Sinnhuber, B.-M., Spelten, N., Strobel, J., Tomsche, L., Turhal, K., van Luijt, R., Versick, S., Voigt, C., Volk, M., von Hobe, M., Weyland, F., Zahn, A., Ziereis, H., and Zlotos, L. O.: Long-range transport of polluted Asian summer monsoon air to high latitudes during the PHILEAS campaign in the boreal summer 2023, Bulletin of the American Meteorological Society, BAMS-D-24-0232.0231, https://doi.org/10.1175/BAMS-D-24-0232.1, 2025.

Roeckner, E., Brokopf, R., Esch, M., Giorgetta, M., Hagemann, S., Kornblueh, L., Manzini, E., Schlese, U., and Schulzweida, U.: Sensitivity of simulated climate to horizontal and vertical resolution in the ECHAM5 atmosphere model, J. Climate, 19, 3771-3791, doi:10.1175/jcli3824.1, 2006.

Rosanka, S., Franco, B., Clarisse, L., Coheur, P. F., Pozzer, A., Wahner, A., and Taraborrelli, D.: The impact of organic 5 pollutants from Indonesian peatland fires on the tropospheric and lower stratospheric composition, Atmos. Chem. Phys., 21, 11257-11288, 10.5194/acp-21-11257-2021, 2021.

Sander, R., Baumgaertner, A., Gromov, S., Harder, H., Jöckel, P., Kerkweg, A., Kubistin, D., Regelin, E., Riede, H., Sandu, A., Taraborrelli, D., Tost, H., and Xie, Z. Q.: The atmospheric chemistry box model CAABA/MECCA-3.0, Geosci. Model Dev., 4, 373–380, 10.5194/gmd-4-373-2011, 2011.

10 Sander, R., Baumgaertner, A., Cabrera-Perez, D., Frank, F., Gromov, S., Grooß, J. U., Harder, H., Huijnen, V., Jöckel, P., Karydis, V. A., Niemeyer, K. E., Pozzer, A., Riede, H., Schultz, M. G., Taraborrelli, D., and Tauer, S.: The community atmospheric chemistry box model CAABA/MECCA-4.0, Geosci. Model Dev., 12, 1365-1385, 10.5194/gmd-12-1365-2019, 2019.

Santee, M. L., Manney, G. L., Livesey, N. J., Schwartz, M. J., Neu, J. L., and Read, W. G.: A comprehensive overview of the 15 climatological composition of the Asian summer monsoon anticyclone based on 10 years of Aura Microwave Limb Sounder measurements, Journal of Geophysical Research: Atmospheres, 122, 5491-5514, 10.1002/2016jd026408, 2017.

Santoso, A., McPhaden, M. J., and Cai, W. J.: The Defining Characteristics of ENSO Extremes and the Strong 2015/2016 El Nino, Reviews of Geophysics, 55, 1079-1129, 10.1002/2017rg000560, 2017.

Schallock, J., Brühl, C., Bingen, C., Höpfner, M., Rieger, L., and Lelieveld, J.: Reconstructing volcanic radiative forcing since 20 1990, using a comprehensive emission inventory and spatially resolved sulfur injections from satellite data in a chemistry-climate model, Atmos. Chem. Phys., 23, 1169-1207, 10.5194/acp-23-1169-2023, 2023.

Seinfeld, J. H., and Pandis, S. N.: Atmospheric Chemistry and Physics: From Air Pollution to Climate Change (Second Edition), John Wiley & Sons. Inc., Hoboken, New Jersey, 2006.

Singer, C. E., Clouser, B. W., Khaykin, S. M., Krämer, M., Cairo, F., Peter, T., Lykov, A., Rolf, C., Spelten, N., Afchine, A., 25 Brunamonti, S., and Moyer, E. J.: Intercomparison of upper tropospheric and lower stratospheric water vapor measurements over the Asian Summer Monsoon during the StratoClim campaign, Atmos. Meas. Tech., 15, 4767-4783, 10.5194/amt-15-4767-2022, 2022.

Smith, W. P., Pan, L. L., Ueyama, R., Honomichl, S., Campos, T., Viciani, S., D'Amato, F., Bianchini, G., Barruci, M., Hornbrook, R. S., Apel, E. C., Hills, A. J., Barletta, B., Atlas, E., Schauffler, S., Treadaway, V., Smith, K., Lueb, R., 30 Hendershot, R., Donnelly, S., Rollins, A., Waxman, E., Novak, G., Huey, L. G., Tanner, D., Lee, Y. R., Bekemeier, C., and Bowman, K. P.: Transport by Asian Summer Monsoon Convection to the Upper Troposphere and Lower Stratosphere During ACCLIP (2022), Journal of Geophysical Research: Atmospheres, 130, e2024JD042732, https://doi.org/10.1029/2024JD042732, 2025.

Sugimoto, S., and Ueno, K.: Formation of mesoscale convective systems over the eastern Tibetan Plateau affected by plateau-scale heating contrasts, Journal of Geophysical Research: Atmospheres, 115, https://doi.org/10.1029/2009JD013609, 2010.

Taraborrelli, D., Lawrence, M. G., Butler, T. M., Sander, R., and Lelieveld, J.: Mainz Isoprene Mechanism 2 (MIM2): an isoprene oxidation mechanism for regional and global atmospheric modelling, Atmos. Chem. Phys., 9, 2751-2777, 10.5194/acp-9-2751-2009, 2009.

Thomason, L. W., and Vernier, J. P.: Improved SAGE II cloud/aerosol categorization and observations of the Asian tropopause aerosol layer: 1989-2005, Atmos. Chem. Phys., 13, 4605-4616, 10.5194/acp-13-4605-2013, 2013.

Thompson, A. M., Pickering, K. E., Dickerson, R. R., Ellis Jr., W. G., Jacob, D. J., Scala, J. R., Tao, W.-K., McNamara, D. P., and Simpson, J.: Convective transport over the central United States and its role in regional CO and ozone budgets, Journal of Geophysical Research: Atmospheres, 99, 18703-18711, https://doi.org/10.1029/94JD01244, 1994.

Thornton, D. C., Bandy, A. R., Blomquist, B. W., Bradshaw, J. D., and Blake, D. R.: Vertical transport of sulfur dioxide and dimethyl sulfide in deep convection and its role in new particle formation, Journal of Geophysical Research: Atmospheres, 102, 28501-28509, https://doi.org/10.1029/97JD01647, 1997.

Tiedtke, M.: A comprehensive mass flux scheme for cumulus parameterization in large-scale models, Mon. Weather Rev., 117, 1779–1800, 1989.

Tomsche, L., Pozzer, A., Ojha, N., Parchatka, U., Lelieveld, J., and Fischer, H.: Upper tropospheric CH4 and CO affected by the South Asian summer monsoon during the Oxidation Mechanism Observations mission, Atmos. Chem. Phys., 19, 1915-1939, 10.5194/acp-19-1915-2019, 2019.

Tost, H., Jöckel, P., Kerkweg, A., Sander, R., and Lelieveld, J.: Technical note: A new comprehensive SCAVenging submodel for global atmospheric chemistry modelling, Atmos. Chem. Phys., 6, 565-574, 10.5194/acp-6-565-2006, 2006a.

Tost, H., Jöckel, P., and Lelieveld, J.: Influence of different convection parameterisations in a GCM, Atmos. Chem. Phys., 6, 5475-5493, 10.5194/acp-6-5475-2006, 2006b.

Tost, H., Jöckel, P., Kerkweg, A., Pozzer, A., Sander, R., and Lelieveld, J.: Global cloud and precipitation chemistry and wet deposition: tropospheric model simulations with ECHAM5/MESSy1, Atmos. Chem. Phys., 7, 2733-2757, 10.5194/acp-7-2733-2007, 2007.

Vernier, H., Rastogi, N., Liu, H., Pandit, A. K., Bedka, K., Patel, A., Ratnam, M. V., Kumar, B. S., Zhang, B., Gadhavi, H., Wienhold, F., Berthet, G., and Vernier, J. P.: Exploring the inorganic composition of the Asian Tropopause Aerosol Layer using medium-duration balloon flights, Atmos. Chem. Phys., 22, 12675-12694, 10.5194/acp-22-12675-2022, 2022.

Vernier, J.-P., Fairlie, T. D., Deshler, T., Ratnam, M. V., Gadhavi, H., Kumar, B. S., Natarajan, M., Pandit, A. K., Raj, S. T. A., Kumar, A. H., Jayaraman, A., Singh, A. K., Rastogi, N., Sinha, P. R., Kumar, S., Tiwari, S., Wegner, T., Baker, N., Vignelles, D., Stenchikov, G., Shevchenko, I., Smith, J., Bedka, K., Kesarkar, A., Singh, V., Bhate, J., Ravikiran, V., Rao, M. D., Ravindrababu, S., Patel, A., Vernier, H., Wienhold, F. G., Liu, H., Knepp, T. N., Thomason, L., Crawford, J., Ziemba, L., Moore, J., Crumeyrolle, S., Williamson, M., Berthet, G., Jégou, F., and Renard, J.-B.: BATAL: The Balloon

Measurement Campaigns of the Asian Tropopause Aerosol Layer, Bulletin of the American Meteorological Society, 99, 955-973, 10.1175/bams-d-17-0014.1, 2018.

Vernier, J. P., Thomason, L. W., and Kar, J.: CALIPSO detection of an Asian tropopause aerosol layer, Geophys. Res. Lett., 38, L07804, 10.1029/2010gl046614, 2011.

5   Vernier, J. P., Fairlie, T. D., Natarajan, M., Wienhold, F. G., Bian, J., Martinsson, B. G., Crumeyrolle, S., Thomason, L. W., and Bedka, K. M.: Increase in upper tropospheric and lower stratospheric aerosol levels and its potential connection with Asian pollution, Journal of Geophysical Research: Atmospheres, 120, 1608-1619, 10.1002/2014jd022372, 2015.

Vogel, B., Günther, G., Müller, R., Grooß, J. U., Hoor, P., Krämer, M., Müller, S., Zahn, A., and Riese, M.: Fast transport from Southeast Asia boundary layer sources to northern Europe: rapid uplift in typhoons and eastward eddy shedding of

10   the Asian monsoon anticyclone, Atmos. Chem. Phys., 14, 12745-12762, 10.5194/acp-14-12745-2014, 2014.

Vogel, B., Günther, G., Müller, R., Grooß, J. U., and Riese, M.: Impact of different Asian source regions on the composition of the Asian monsoon anticyclone and of the extratropical lowermost stratosphere, Atmos. Chem. Phys., 15, 13699-13716, 10.5194/acp-15-13699-2015, 2015.

Vogel, B., Günther, G., Müller, R., Grooß, J. U., Afchine, A., Bozem, H., Hoor, P., Krämer, M., Müller, S., Riese, M., Rolf,

15   C., Spelten, N., Stiller, G. P., Ungermann, J., and Zahn, A.: Long-range transport pathways of tropospheric source gases originating in Asia into the northern lower stratosphere during the Asian monsoon season 2012, Atmos. Chem. Phys., 16, 15301-15325, 10.5194/acp-16-15301-2016, 2016.

Vogel, B., Volk, C. M., Wintel, J., Lauther, V., Müller, R., Patra, P. K., Riese, M., Terao, Y., and Stroh, F.: Reconstructing high-resolution in-situ vertical carbon dioxide profiles in the sparsely monitored Asian monsoon region, Communications

20   Earth & Environment, 4, 72, 10.1038/s43247-023-00725-5, 2023.

Vogel, B., Lauther, V., Köllner, F., Ekinci, F., Rolf, C., Strobel, J., van Luijt, R., Volk, M. C., Borrmann, S., Dragoneas, A., Eppers, O., Molleker, S., Hoor, P., Ort, L., Weyland, F., Zahn, A., Clemens, J., Günther, G., Kachula, O., Müller, R., Ploeger, F., and Riese, M.: Continental and marine source regions contributing to the outflow of the Asian summer monsoon anticyclone during the PHILEAS campaign in summer 2023, EGUsphere, 2025, 1-49, 10.5194/egusphere-2025-

25   5609, 2025.

von Hobe, M., Ploeger, F., Konopka, P., Kloss, C., Ulanowski, A., Yushkov, V., Ravegnani, F., Volk, C. M., Pan, L. L., Honomichl, S. B., Tilmes, S., Kinnison, D. E., Garcia, R. R., and Wright, J. S.: Upward transport into and within the Asian monsoon anticyclone as inferred from StratoClim trace gas observations, Atmos. Chem. Phys., 21, 1267-1285, 10.5194/acp-21-1267-2021, 2021.

30   Wang, B., and LinHo: Rainy Season of the Asian–Pacific Summer Monsoon, Journal of Climate, 15, 386-398, https://doi.org/10.1175/1520-0442(2002)015<0386:RSOTAP>2.0.CO;2, 2002.

Wang, T., Song, Y., Xu, Z., Liu, M., Xu, T., Liao, W., Yin, L., Cai, X., Kang, L., Zhang, H., and Zhu, T.: Why is the Indo-Gangetic Plain the region with the largest NH3 column in the globe during pre-monsoon and monsoon seasons?, Atmos. Chem. Phys., 20, 8727-8736, 10.5194/acp-20-8727-2020, 2020.

Xenofontos, C., Kohl, M., Ruhl, S., Almeida, J., Beckmann, H. M., Caudillo-Plath, L., Ehrhart, S., Höhler, K., Kaniyodical Sebastian, M., Kong, W., Kunkler, F., Onnela, A., Rato, P., Russell, D. M., Simon, M., Stark, L., Umo, N. S., Unfer, G. R., Yang, B., Yu, W., Zauner-Wieczorek, M., Zgheib, I., Zheng, Z., Curtius, J., Donahue, N. M., El Haddad, I., Flagan, R. C., Gordon, H., Harder, H., He, X.-C., Kirkby, J., Kulmala, M., Möhler, O., Pöhlker, M. L., Schobesberger, S., Volkamer, R., Wang, M., Borrmann, S., Pozzer, A., Lelieveld, J., and Christoudias, T.: The impact of ammonia on particle formation in the Asian Tropopause Aerosol Layer, npj Climate and Atmospheric Science, 7, 215, 10.1038/s41612-024-00758-3, 2024.

Xenofontos, C., Kohl, M., Ruhl, S., Almeida, J., Caudillo-Plath, L., Cruz-Simbron, R., Dada, L., Duplissy, J., Ehrhart, S., Finkenzeller, H., Höhler, K., Kong, W., Kunkler, F., Lietzke, C. J., Mentler, B., Morawiec, A., Onnela, A., Rato, P., Rörup, B., Russell, D. M., Schervish, M., Scholz, W., Sebastian, M. K., Simon, M., Sommer, E., Tong, Y., Umo, N. S., Unfer, G. R., Vettikkat, L., Yang, B., Yu, W., Zgheib, I., Zheng, Z., Curtius, J., Donahue, N. M., Flagan, R. C., Gordon, H., El Haddad, I., Hansel, A., Harder, H., He, X.-C., Kirkby, J., Kulmala, M., Lehtipalo, K., Möhler, O., Petäjä, T., Pöhlker, M. L., Schobesberger, S., Stolzenburg, D., Wang, M., Winkler, P. M., Worsnop, D. R., Höpfner, M., Volkamer, R., Pozzer, A., Lelieveld, J., and Christoudias, T.: Global impact of anthropogenic NH_3 emissions on upper tropospheric aerosol formation, Proceedings of the National Academy of Sciences, 122, e2506658122, doi:10.1073/pnas.2506658122, 2025.

Xu, X., Zhao, T., Lu, C., Guo, Y., Chen, B., Liu, R., Li, Y., and Shi, X.: An important mechanism sustaining the atmospheric "water tower" over the Tibetan Plateau, Atmos. Chem. Phys., 14, 11287-11295, 10.5194/acp-14-11287-2014, 2014.

Yan, X., Konopka, P., Ploeger, F., Tao, M., Müller, R., Santee, M. L., Bian, J., and Riese, M.: El Niño Southern Oscillation influence on the Asian summer monsoon anticyclone, Atmos. Chem. Phys., 18, 8079-8096, 10.5194/acp-18-8079-2018, 2018.

Yang, Q., Easter, R. C., Campuzano-Jost, P., Jimenez, J. L., Fast, J. D., Ghan, S. J., Wang, H., Berg, L. K., Barth, M. C., Liu, Y., Shrivastava, M. B., Singh, B., Morrison, H., Fan, J., Ziegler, C. L., Bela, M., Apel, E., Diskin, G. S., Mikoviny, T., and Wisthaler, A.: Aerosol transport and wet scavenging in deep convective clouds: A case study and model evaluation using a multiple passive tracer analysis approach, Journal of Geophysical Research: Atmospheres, 120, 8448-8468, doi:10.1002/2015JD023647, 2015.

Yienger, J. J., and Levy II, H.: Empirical model of global soil-biogenic NO_x emissions, Journal of Geophysical Research: Atmospheres, 100, 11447-11464, doi:10.1029/95JD00370, 1995.

Yu, P., Rosenlof, K. H., Liu, S., Telg, H., Thornberry, T. D., Rollins, A. W., Portmann, R. W., Bai, Z., Ray, E. A., Duan, Y., Pan, L. L., Toon, O. B., Bian, J., and Gao, R.-S.: Efficient transport of tropospheric aerosol into the stratosphere via the Asian summer monsoon anticyclone, Proceedings of the National Academy of Sciences, 114, 6972–6977, 10.1073/pnas.1701170114, 2017.

Zhou, X., Lou, C., Li, W. L., and Shi, J. E.: Ozone changes over China and low center over Tibetan Plateau, Chin. Sci. Bull., 40, 1396-1398, 1995.

Zondlo, M. A., Barone, S. B., and Tolbert, M. A.: Uptake of HNO$_3$ on ice under upper tropospheric conditions, Geophysical
   Research Letters, 24, 1391-1394, https://doi.org/10.1029/97GL01287, 1997.

5
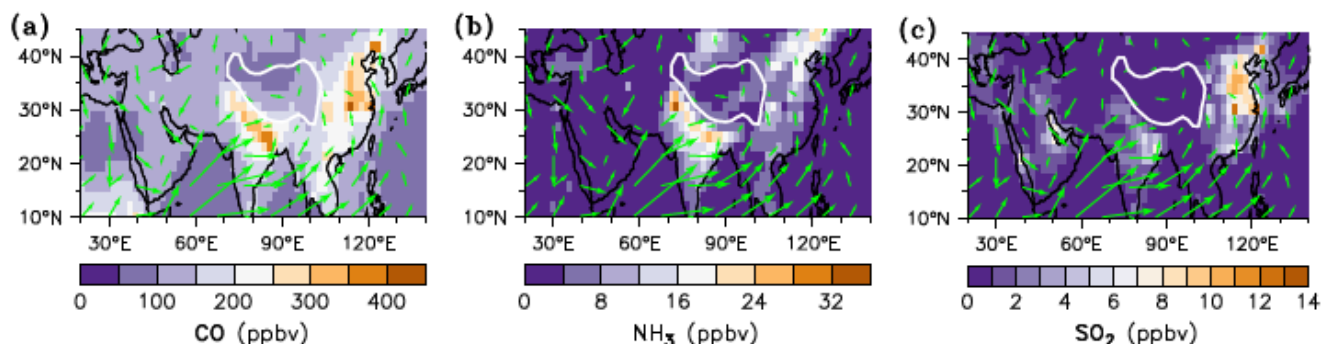
Figure 1. EMAC simulated volume mixing ratios of CO **(a)**, NH$_3$ **(b)** and SO$_2$ **(c)** overlaid with the wind vectors in the PBL, averaged for JJA over the years 2010-2020. White lines represent the 3 km terrain height contour, highlighting the Tibetan Plateau.
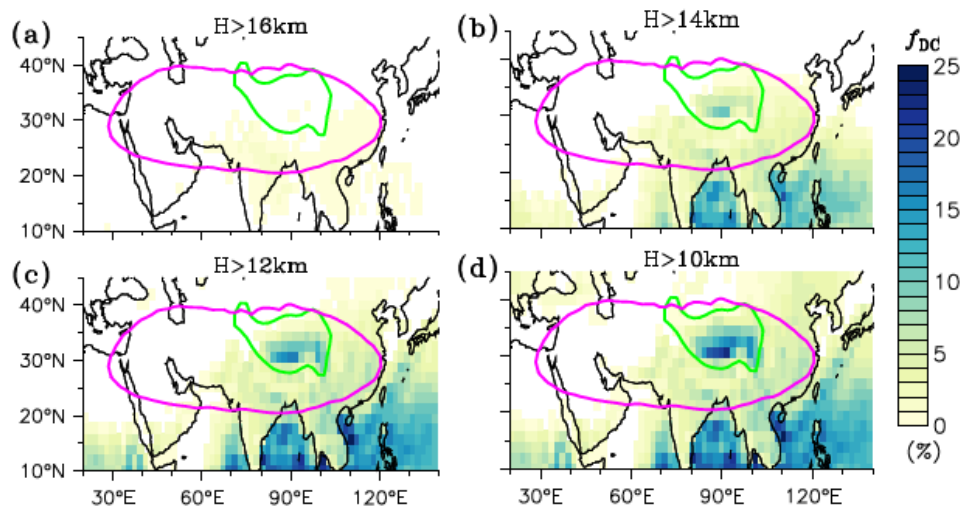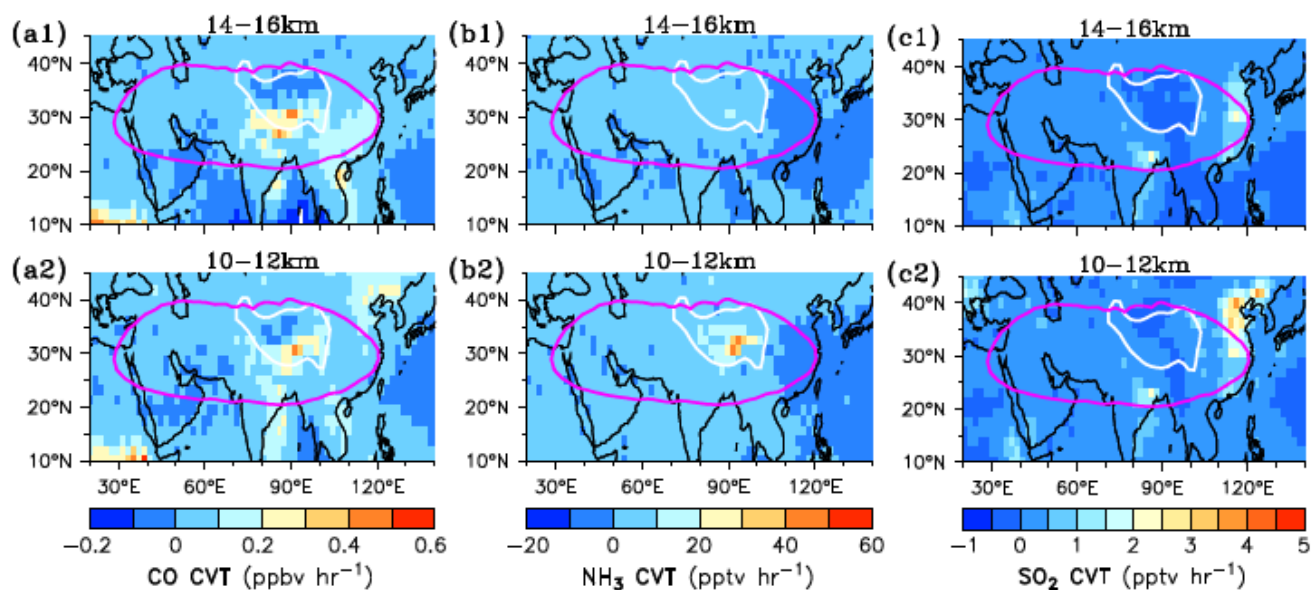

Figure 2. EMAC simulated relative deep convection frequency (f_{DC} in percent) for selected convective cloud top heights, i.e., above 16 km **(a)**, 14 km **(b)** 12 km **(c)**, and 10 km **(d)** above sea level, in JJA during the years 2010-2020. Purple lines are the 16.64 km geopotential height contour at 100 hPa, highlighting the main ASMA area (see Figure S1). Green lines represent the 3 km terrain height contour, highlighting the Tibetan Plateau.
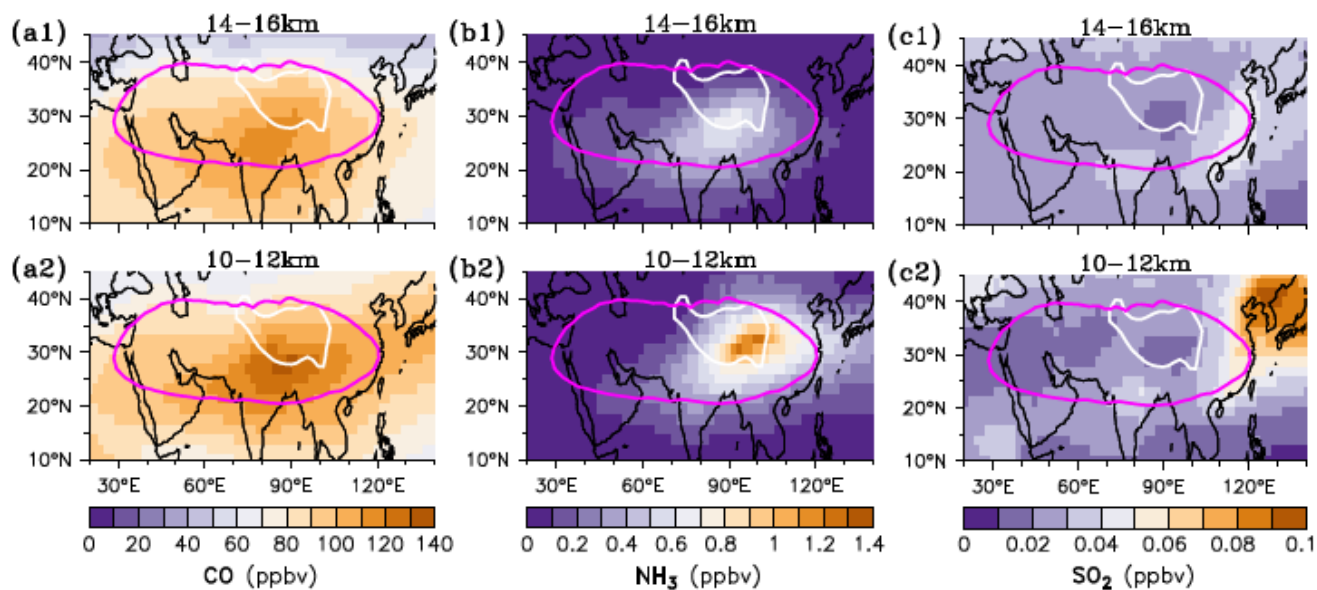
Figure 3. EMAC simulated volume mixing ratios of CO (**a1** and **a2**), NH$_3$ (**b1** and **b2**) and SO$_2$ (**c1** and **c2**) at selected altitudes, i.e., 14-16 km (**a1**, **b1** and **c1**) and 10-12 km (**a2**, **b2** and **c2**) above sea level, averaged for JJA over the years 2010-2020. Purple lines show the 16.64 km geopotential height contour at 100 hPa, highlighting the main ASMA area (see Figure S1). White lines represent the 3 km terrain height contour, highlighting the Tibetan Plateau.

.

Figure 4. EMAC simulated mean deep convective transport tendency (CVT) of CO (**a1** and **a2**), NH$_3$ (**b1** and **b2**) and SO$_2$ (**c1** and **c2**) at selected altitudes, i.e., 14-16 km (**a1**, **b1** and **c1**) and 10-12 km (**a2**, **b2** and **c2**) above sea level, averaged for JJA over the years 2010-2020. Purple lines show the 16.64 km geopotential height contour at 100 hPa, highlighting the main ASMA area (see Figure S1). White lines represent the 3 km terrain height contour, highlighting the Tibetan Plateau.

3
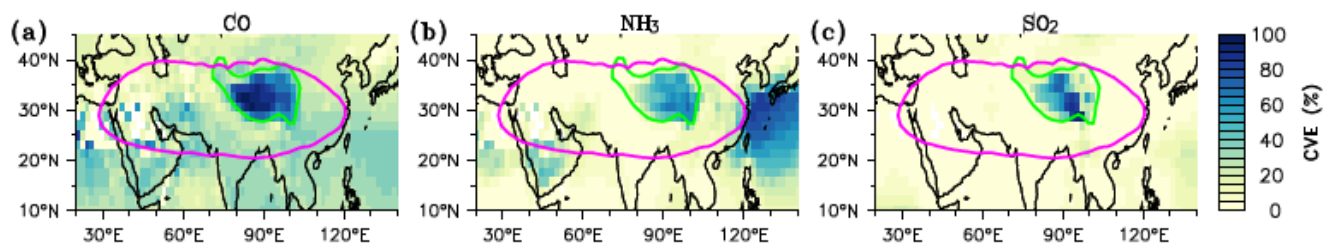
Figure 5. EMAC simulated mean deep convective transport efficiency (CVE), i.e., the ratio of the updraft mass flux (UMF) at 10 km height above sea level to its maximum in the deep convection column (expressed in percent), for CO **(a)**, NH$_3$ **(b)** and SO$_2$ **(c)**, in JJA during the years 2010-2020. Purple lines show the 16.64 km geopotential height contour at 100 hPa, highlighting the main ASMA area (see Figure S1). Green lines represent the 3 km terrain height contour, highlighting the Tibetan Plateau.
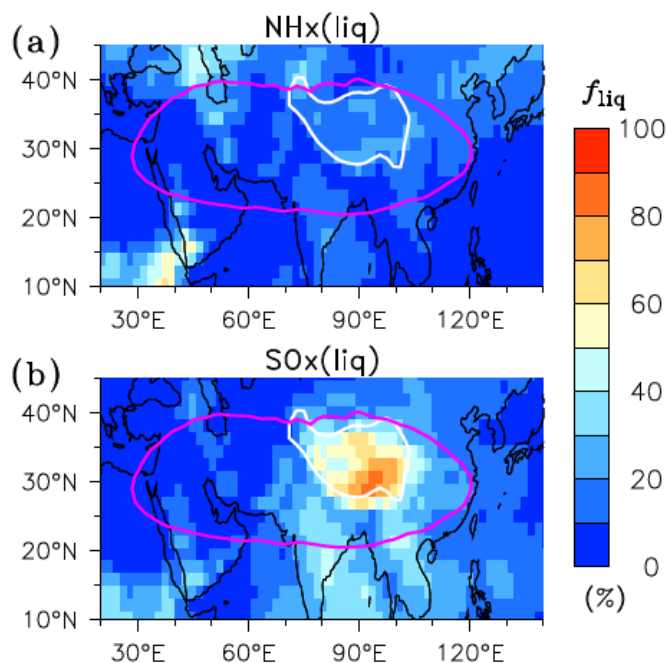
Figure 6. EMAC simulated mean relative contributions of the liquid-phase amount to the total (gas-phase plus liquid-phase) within a vertical column of 6-10 km above sea level (f_{liq}), for NH$_3$ and its reaction products in the clouds (denoted by NHx) **(a)** and SO$_2$ and its reaction products in the clouds (denoted by SOx) **(b)**, in JJA during the years 2010-2020. Purple lines show the 16.64 km geopotential height contour at 100 hPa, highlighting the main ASMA area (see Figure S1). White lines represent the 3 km terrain height contour, highlighting the Tibetan Plateau.

4
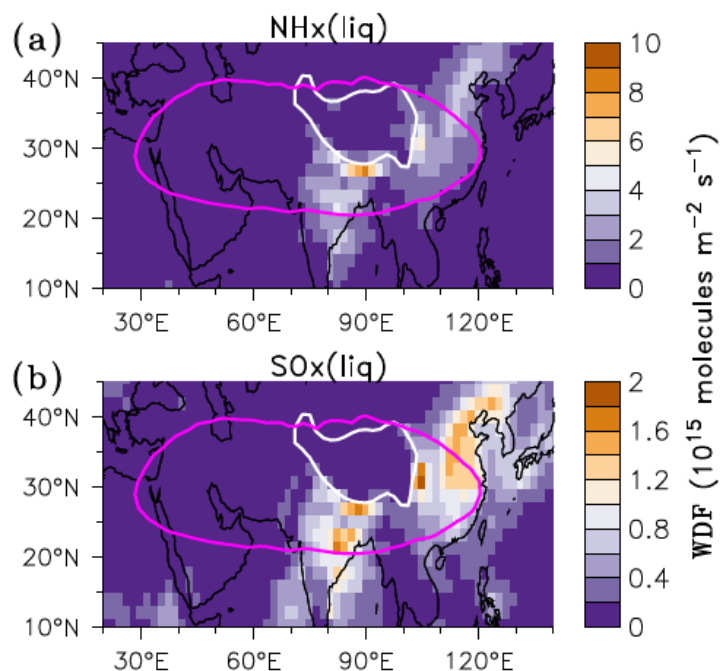
Figure 7. EMAC simulated wet deposition fluxes (WDF) of NH$_3$ and its reaction products in the rains (denoted by NHx) (**a**) and SO$_2$ and its reaction products in the rains (denoted by SOx) (**b**), averaged for JJA over the years 2010-2020. Purple lines show the 16.64 km geopotential height contour at 100 hPa, highlighting the main ASMA area (see Figure S1). White lines represent the 3 km terrain height contour, highlighting the Tibetan Plateau.
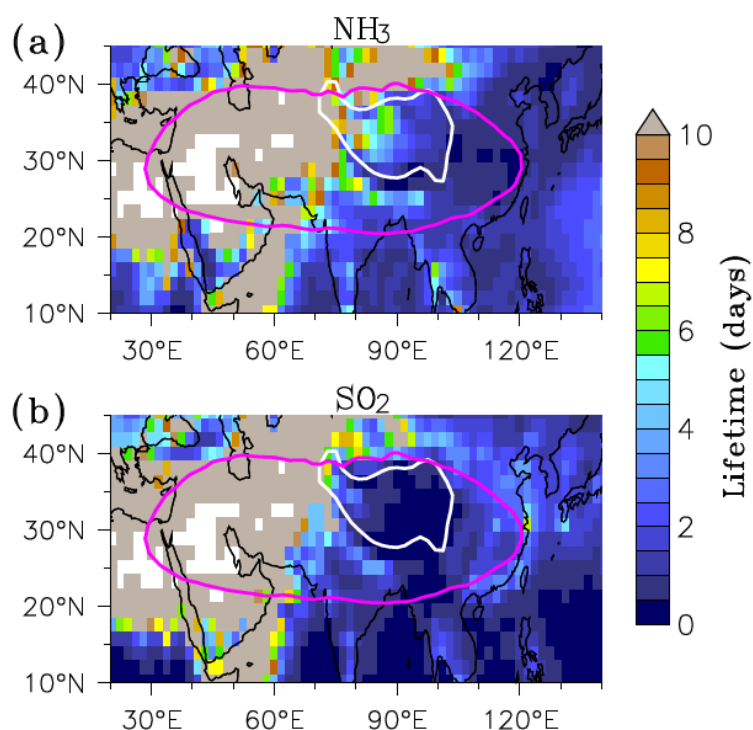
Figure 8. EMAC simulated mean atmospheric lifetimes of tropospheric NH_3 **(a)** and SO_2 **(b)** (below 10 km height above sea level) against wet deposition in JJA during the years 2010-2020. Purple lines show the 16.64 km geopotential height contour at 100 hPa, highlighting the main ASMA area (see Figure S1). White lines represent the 3 km terrain height contour, highlighting the Tibetan Plateau.